Published in final edited form as:

Mol Cell. 2023 June 15; 83(12): 2059–2076.e6. doi:10.1016/j.molcel.2023.05.031.

A mitochondrial iron-responsive pathway regulated by DELE1

Yusuke Sekine[1,2,#], **Ryan Houston**[1,#], **Eva-Maria Eckl**[3], **Evelyn Fessler**[3], **Derek P Narendra**[4], **Lucas T Jae**[3], **Shiori Sekine**[1,5,*]

[1]Aging Institute, Department of Medicine, School of Medicine, University of Pittsburgh, Pittsburgh, PA, USA, 15219

[2]Division of Endocrinology and Metabolism, Department of Medicine, School of Medicine, University of Pittsburgh, Pittsburgh, PA, USA, 15213

[3]Gene Center and Department of Biochemistry, Ludwig-Maximilians-Universität München, Munich, Germany, 81377

[4]Inherited Movement Disorders Unit, Neurogenetics Branch, National Institute of Neurological Disorders and Stroke, National Institutes of Health, Bethesda, MD, USA, 20814

[5]Division of Cardiology, Department of Medicine, School of Medicine, University of Pittsburgh, Pittsburgh, PA, USA, 15213

Summary

The heme-regulated kinase HRI is activated under heme/iron deficient conditions; however, the underlying molecular mechanism is incompletely understood. Here, we show that iron deficiency-induced HRI activation requires the mitochondrial protein DELE1. Notably, mitochondrial import of DELE1 and its subsequent protein stability are regulated by iron availability. Under steady state conditions, DELE1 is degraded by the mitochondrial matrix-resident protease LONP1 soon after mitochondrial import. Upon iron chelation, DELE1 import is arrested, thereby stabilizing DELE1 on the mitochondrial surface to activate the HRI-mediated integrated stress response (ISR). Ablation of this DELE1-HRI-ISR pathway in an erythroid cell model enhances cell death under iron-limited conditions, suggesting a cell protective role for this pathway in iron-demanding cell lineages. Our findings highlight mitochondrial import regulation of DELE1 as the core component of a previously unrecognized mitochondrial iron responsive pathway that elicits stress signaling following perturbation of iron homeostasis.

* Lead contact, Shiori Sekine, Mailing address: Bridgeside Point 1, Room 568, 100 Technology Drive, Pittsburgh, PA 15219, Phone: 412-383-0867, sekine@pitt.edu.

#These authors contributed equally.

Author contributions

S.S. led the project. Y.S., R.H., E.E., E.F., D.P.N. and S.S. designed and performed experiments. D.P.N. and L.T.J. supported the project by providing supervision, suggestions and reagents. Y.S. and S.S. wrote an initial draft of the manuscript. All the authors edited the manuscript.

Declaration of interests

The authors declare no competing financial interest.

eTOC blurb

Sekine and Houston et al. identified DELE1 as an iron-responsive molecule at mitochondria that has cell protective roles via HRI-ISR pathway activation in iron-deficient conditions. The mitochondrial import and subsequent degradation of DELE1 were regulated by intracellular iron availability, demonstrating the general importance of import coupled-stress sensing mechanisms at mitochondria.

Graphical Abstract

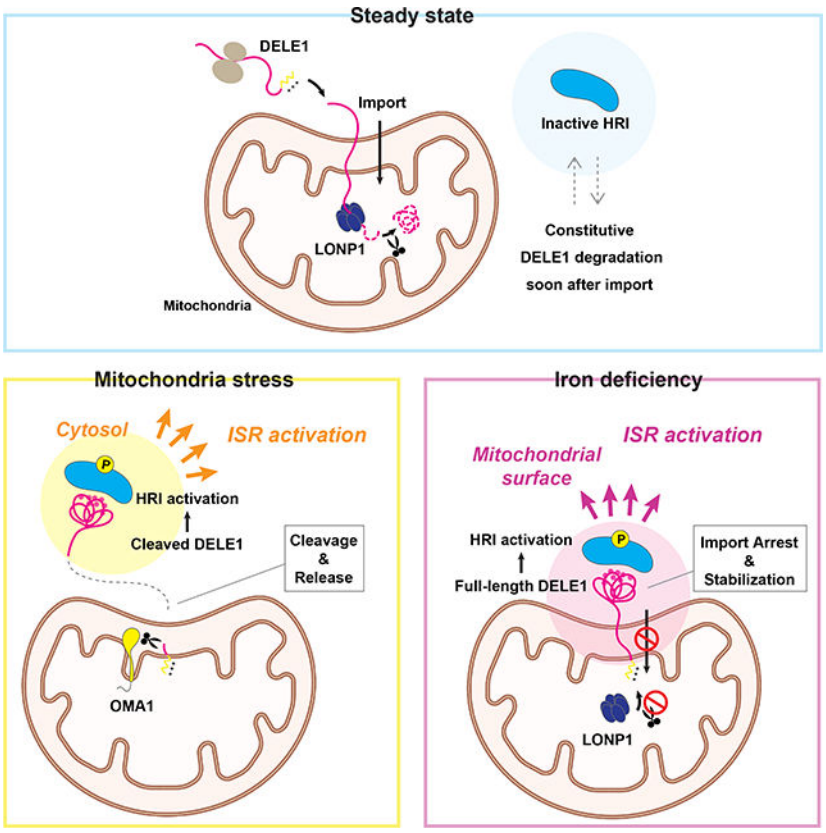

Keywords

HRI; DELE1; LONP1; integrated stress response; iron; mitochondria; mitochondrial import; mitochondrial proteostasis; erythroid cells

Introduction

The cytosolic kinase HRI is highly expressed in erythroid cells and governs the stress response called integrated stress response (ISR) during terminal erythropoiesis[1–3]. Under stress conditions, HRI phosphorylates the α subunit of the translation initiation factor eIF2 (eIF2α), thereby attenuating global mRNA translation, while activating the transcription factor ATF4, a master regulator of the transcriptional response for the ISR. Early studies using rabbit reticulocyte lysates revealed that the addition of hemin (heme) to the lysates

reverses HRI-mediated translational inhibition [4–7]. Subsequent *in vitro* studies using purified HRI demonstrated that the direct binding of heme on HRI modulated the conformation of HRI thereby suppressing its kinase activity [8–11]. These findings led to a current model of HRI regulation in which HRI is activated through dissociation of the inhibitory heme from HRI when intracellular levels of heme decline. HRI knockout (KO) mice do not exhibit significant erythroid abnormalities under standard dietary condition [12]. However, when challenged with an iron deficient diet, these mice develop a characteristic anemia with globin aggregation in red blood cells [12]. One potential explanation for these iron-dependent *in vivo* effects is that iron deficiency concomitantly decreases heme levels, and this fall in heme is the mechanism of HRI activation. However, such conjectures have remained unproven.

It has been shown that various types of mitochondrial stress, such as membrane potential loss, inhibition of OXPHOS, and perturbation of mitochondrial proteostasis, activate the ISR [13–15]. Recent cell genetic screens have demonstrated that HRI is required for the mitochondrial stress-triggered ISR activation, and identified the mitochondria resident proteins DELE1 and OMA1 as upstream regulators of HRI [16,17]. Upon treatment with various mitochondrial stressors the mitochondrial protease OMA1 cleaves DELE1, and the cleaved form of DELE1 is released into the cytosol where it interacts with HRI, activating the ISR. Recent studies have indicated the importance of this pathway in *in vivo* models of mitochondrial cardiomyopathy [18–21]. However, the functional link between this newly identified mitochondria-dependent pathway and the classic heme-dependent HRI regulation model remains unclear.

Accumulating evidence indicates that mitochondrial import of certain proteins is precisely regulated in response to mitochondrial stress. Importantly, this regulation is often used to signal mitochondrial stress to other subcellular compartments such as the cytosol and the nucleus, which constitutes the “mitochondrial import-coupled stress response”. A well characterized example of this is the Parkinson’s Disease (PD)-linked mitochondrial kinase PINK1, whose import arrest and stabilization on the outer mitochondrial membrane (OMM) upon mitochondrial depolarization triggers Parkin-mediated mitophagy [22–24]. Furthermore, it has been shown in *C. elegans* that suppression of the mitochondrial import of the transcription factor ATFS-1 by proteotoxic stress leads to the translocation of ATFS-1 to the nucleus, which is central for the transcriptional response known as the mitochondrial unfolded protein response (mtUPR) [25].

Here, we show another example of the mitochondrial import-coupled stress response. We found that DELE1 is an iron responsive protein whose mitochondrial import and subsequent protein stability are regulated by intracellular iron availability. The full-length form of DELE1, stabilized by iron deficiency, interacted with and activated HRI on the mitochondrial surface, suggesting that mitochondria are utilized as a site for triggering the ISR when iron homeostasis is perturbed. Our findings point to a hitherto unappreciated mitochondrial-based iron-monitoring system and also underscore the importance of mitochondrial protein import regulation as a dynamic, stress-sensing mechanism.

Results

DELE1 is a short-lived protein that is degraded by LONP1 after mitochondrial import

Previous studies have suggested that the protein stability of DELE1 is post-translationally regulated in cultured cells [26,27]. To monitor endogenous DELE1 protein stability, we performed cycloheximide (CHX)-chase experiments using HEK293T cells expressing an endogenously HA-tagged DELE1, which overcame the difficulty of detecting endogenous DELE1 using the currently available antibodies [16,17]. Consistent with the recent study [27], DELE1 underwent rapid degradation within minutes of CHX treatment (Figure 1A). In contrast, expression levels of other mitochondrial proteins such as TOM40, TIM50 and TIM23 did not change during this chase period (Figure 1A). This suggests that DELE1 is actively degraded under basal conditions. The proteasome inhibitor MG132 and the autophagy inhibitor Bafilomycin A1 did not enhance DELE1 expression (Figure 1B), while these inhibitors accumulated their known substrates (the cleaved form of PINK1 for the proteasome and p62 for autophagy) [22,28], indicating that DELE1 is likely degraded independent of the proteasome and macroautophagy. We thus speculated that mitochondrial proteases may be involved in its basal degradation and conducted a small scale screen using siRNAs for reported mitochondrial proteases (Figures 1C and 1D) [29]. This targeted screen found that knockdown of LONP1, the matrix-localized ATP-dependent serine protease [30], had the most pronounced effects on DELE1 (Figure 1D). LONP1 siRNAs increased DELE1 at steady state, and almost completely prevented DELE1 degradation during the CHX-chase (Figure 1E). We also observed partial restoration of DELE1 expression in cells with knockdown of AFG3L2 and SPG7, that comprise the matrix-facing m-AAA protease (Figure 1D) [29]. In contrast, none of the siRNAs for the inner mitochondrial membrane (IMM) or intermembrane space (IMS) proteases affected DELE1 stability (Figure 1C). These observations suggest that DELE1 is degraded in the mitochondrial matrix predominantly in a LONP1-dependent manner.

Iron deficiency stabilizes DELE1

LONP1 is known to function as a quality control protease that degrades misfolded and oxidatively damaged proteins in the mitochondrial matrix [30]. It has also been shown that LONP1 is actively involved in various mitochondrial processes through the regulated proteolysis of specific substrates. Considering that DELE1 is an activator of the heme-responsive kinase HRI, we tested whether heme and iron-related stimuli affected LONP1-mediated degradation of DELE1. We found that two iron chelators, deferoxamine (DFO) and deferiprone (DFP) increased DELE1 protein levels (Figure 2A). These compounds have been shown to decrease both cytosolic and mitochondrial iron levels [31,32], and we confirmed their effects by monitoring the increase in the cytosolic iron-responsive protein IRP2 [33] (Figure 2A). In contrast, neither heme (hemin) nor a heme biosynthesis inhibitor (succinyl acetone, SA) affected DELE1 expression, while the heme-responsive proteins ALAS1 and HMOX1 were increased by SA and hemin, respectively (Figure 2A). Whereas the mitochondrial uncoupler CCCP induced the cleavage of DELE1 as previously reported [16,17], DFO and DFP treatment appeared to promote stabilization of DELE1, including its full-length form (Figure 2A). Levels of a tetracycline (tet)-inducible DELE1-HA in HeLa cells was also enhanced in a DFO dose-dependent manner, similar to the response

of IRP2 (Figure 2B). CHX-chase experiments revealed that pre-treatment with DFO or DFP significantly stabilized the full-length form of endogenous DELE1 following a CHX-chase (Figure 2C). This was also observed for exogenously expressed DELE1-HA in DELE1 KO HEK293T cells (Figures 2D and S1A). In contrast, pre-treatment with CCCP stabilized DELE1, but as the cleaved form (Figure 2C). It is noteworthy that for unknown reasons, the iron deficiency-induced accumulation of endogenously HA-tagged DELE1 was more prominently observed when cells were seeded at a lower cell density (Figure S1B). Nevertheless, CHX-chase experiments clearly demonstrate that under iron-deficient conditions, DELE1 is stabilized at any cell density (Figure S1B). Collectively, this implies that full-length DELE1 stability is regulated by iron availability.

DELE1 has a predicted mitochondrial targeting sequence (MTS) at its N-terminus and the MTS cleavage site is predicted to be located after amino acid 23 by the web tool MitoFates (Figure 2E) [34], which has been experimentally verified [27]. We confirmed that tet-induced DELE1 wild-type (WT) is localized to mitochondria (Figure 2E). Consistent with previous reports [16,17], a DELE1 mutant that lacked the predicted MTS (DELE1 d30) partially prevented mitochondrial localization of DELE1, but deletion of the N-terminal 101 amino acids of DELE1 (DELE1 d101) almost completely blocked mitochondrial localization (Figure 2E). These results suggest that mitochondrial localization of DELE1 is regulated by a longer N-terminal region encompassing the predicted MTS. Unlike DELE1 WT, the DELE1 d101 mutant lost the ability to accumulate in response to iron chelation (Figure 2F), suggesting that DELE1 responds to iron deficiency at mitochondria.

DELE1 is stabilized on mitochondria by an iron deficiency-dependent mitochondrial import arrest

Treatment of iron chelators significantly decreased mitochondrial ISC-containing proteins including SDHB and LIAS (Figure S2A), suggesting that iron deprivation affected the mitochondrial ISC biosynthesis pathway. It has been reported that misfolded SDHB due to the failure of ISC insertion undergoes degradation by LONP1 [35]. Indeed, LONP1 knockdown restored the expression of SDHB as well as that of LIAS in iron-chelated cells (Figure S2A), suggesting that LONP1 mediates the degradation of these ISC proteins. Thus, it appears that LONP1 is still active for degrading misfolded ISC proteins under iron deficient conditions, although DELE1 appears to escape from LONP1-mediated degradation.

CCCP treatment induces cleavage of DELE1 by OMA1 and that cleaved DELE1 is released into the cytosol [16,17]. We confirmed this observation in our tet-on DELE1-HA HeLa cells (Figure 3A). In contrast, we found that DELE1 was detected predominantly on mitochondria after treatment with DFO (Figure 3A), indicating that DELE1 does not substantially translocate to the cytosol during iron deficiency. This is consistent with the observation that unlike CCCP, iron chelators do not induce cleavage of DELE1 to the same extent as CCCP but rather stabilizes the full-length form of DELE1 (Figures 2A–2C). Cell fractionation analysis of HEK293T cells expressing endogenously HA-tagged DELE1 also revealed that in iron-deficient conditions, the stabilized, full-length DELE1 was retained in the mitochondrial fraction (Figure S2B). Moreover, under iron-deficient conditions, when

cells were subsequently exposed to CCCP, the full-length form of DELE1 was able to be converted into the OMA1-cleaved form, indicating that at least during iron deficiency the OMA1 cleavage site (around reside 142 of DELE1) [17] is located in the IMS (Figure S2C). To further determine the precise localization of DELE1 within mitochondria before and after iron chelation, we performed a protease protection assays after a CHX chase by using crude mitochondria isolated from endogenously HA-tagged DELE1 expressing HEK293T cells (Figure 3B). When de novo protein synthesis was blocked with CHX, the balance of DELE1 shifted in favor of its MPP-cleaved form and it was largely protected from proteinase K in isotonic (SEM) buffer, as expected. In contrast, under iron deficiency, a substantial amount of the stabilized DELE1 showed a higher sensitivity to proteinase K in isotonic buffer (Figure 3B), suggesting that the C-terminal region of these DELE1 is exposed outside of the OMM after iron deficiency. We thus hypothesized that the mitochondrial import of DELE1 may be arrested in response to iron deficiency. To monitor the entrance of the N-terminus of DELE1 into the matrix, the TEV sequence (that is recognized and cleaved by TEV protease) was inserted after the predicted MTS of DELE1 [DELE1(TEV30)] (Figure 3C). We expressed DELE1(TEV30) with or without a matrix-targeted TEV protease (Su9-TEV protease) [36] in DELE1 KO HEK293T cells, and subsequently treated the cells with DFO. In the absence of Su9-TEV protease, the N-terminal MTS of DELE1 should be cleaved by the endogenous MTS-cleaving peptidase (MPP) in the matrix [27]. In the presence of Su9-TEV protease, the N-terminal 36 amino acids of DELE1 should be cleaved by Su9-TEV protease (Figure 3C). Indeed, DELE1(TEV30) appeared as a doublet under steady state conditions when resolved on an SDS-PAGE 7.5% acrylamide gel; the upper band was the full-length form and the lower band was either the MPP- or TEV-cleaved form (Figures 3D and S2D). Following iron chelation with DFO, cleavage of DELE(TEV30)-HA by matrix MPPs or TEV was partially blocked (Figure 3D). These observations suggest that under iron deficient conditions the N-terminal region of DELE1 reaches the matrix less readily than in the steady state due to mitochondrial import arrest (Figure 3C). By separating endogenous DELE1 protein on SDS-PAGE at high resolution, we also confirmed that iron chelators stabilized the full-length form, but not the MPP-cleaved form of endogenous DELE1, whereas LONP1 knockdown resulted in stabilization of both forms of DELE1 (Figures 3E and 3F). These results suggest that this iron deficiency-induced mitochondrial import arrest of DELE1 may enable DELE1 to escape from MPP-mediated MTS cleavage and subsequent LONP1-mediated degradation, thereby promoting the stabilization of full-length DELE1 (Figure 3C). Although our observations suggested that the stabilized, full-length DELE1 passed through the IMS and OMM (Figures S2C and 3B), stable interactions between DELE1 and TOM/TIM import channels were not observed, in contrast to PINK1 import arrest (Figure S2E) [37–40].

Mitochondrial membrane potential across the IMM provides a driving force for the mitochondrial import of MTS-containing proteins [41]. Consistently, mitochondrial depolarization by CCCP therefore induced the accumulation of the full-length (MPP-uncleaved) form of PINK1 [23,24] and Su9-DHFR, a model protein for MTS-mediated import (Figures 3G and 3H). Although DELE1 is cleaved by OMA1 under CCCP-treated conditions, the total amount of DELE1 protein increased (Figures 2A and 3I). This indicates that like other mitochondrial proteins with a canonical MTS, the mitochondrial import

of DELE1 depends on mitochondrial membrane potential. In contrast, while DELE1 was stabilized by iron deficiency, both PINK1 and Su9-DHFR were insensitive to this perturbation (Figures 3G and 3H). Thus, iron chelation-dependent import arrest is not a general means of regulation for MTS-containing proteins and may be specific for DELE1.

DELE1 activates an HRI-mediated ISR following iron deficiency

We next examined the possibility that stabilized DELE1 in response to iron deficiency activates the HRI-ISR pathway. Treatment with the iron chelators DFO or DFP increased phosphorylation of eIF2α and expression of ATF4 in a time- and concentration-dependent manner (Figures 4A and 4B). Flow cytometric quantitative analyses using an ATF4 reporter indicated DFO-dependent translational upregulation of ATF4 (Figure 4C) [17]. Furthermore, the increase in ATF4 expression was attenuated by ISRIB, a chemical inhibitor of the ISR (Figure S3A) [42,43]. The time course of ATF4 accumulation by iron chelation was slower than that induced by CCCP (Figure 4A). However, ATF4 accumulation followed the induction of IRP2 and was well correlated with the stabilization of DELE1, as well as with the degradation of mitochondrial and cytosolic ISC proteins (Figure S3B). Concomitant iron supplementation using high concentrations of ferric ammonium citrate (FAC) appeared to counteract the effects of cytosolic and mitochondrial iron chelation by DFO, as indicated by suppression of IRP2 accumulation and LIAS degradation, as well as induction of mitochondrial Ferritin (FTMT) (Figure 4D). FAC treatment also abrogated DFO-induced stabilization of endogenous DELE1 and ATF4 activation (Figure 4D). In contrast, the heme biosynthesis inhibitor SA did not activate the ISR at least within the time points investigated (Figure 4E). Addition of hemin to the culture media substantially increased the expression of HMOX1 [44] under DFO-treated conditions, but it did not overcome DFO-induced iron deficiency (monitored by IRP2) (Figure 4F). Under this condition, hemin supplementation less efficiently suppressed the iron chelation-induced stabilization of endogenous DELE1 and accumulation of ATF4 compared to FAC treatment (Figure 4F). Collectively, these results suggest that iron is the primary factor in DFO-induced DELE1 stabilization and ISR activation.

Moreover, knockdown experiments revealed that both HRI and DELE1 were required for DFO and DFP-induced ISR activation in HeLa cells (Figures 4G, S3C and S3D). Genetic ablation of DELE1 by CRISPR-Cas9 genome editing in HEK293 cells (Figure S1A) suppressed iron chelation-induced ATF4 activation (Figures 4H and S3E), as well as the transcriptional activation of classical ISR target genes including *DDIT3*, *ASNS*, *CTH* and *CHAC1* (Figure 4I). Exogenous reconstitution of DELE1 WT rescued the ISR activation in DELE1 KO cells, while this was not observed when a DELE1 mutant lacking the TPR2 domain was expressed (Figure 4J). The latter observation is consistent with previous studies showing that the TRP2 domain of DELE1 is required for activation of HRI under mitochondrial stress [16,17]. Thus, the DELE1-HRI pathway is required for the activation of ISR in iron-deficient cells.

DELE1 on mitochondrial surface activates HRI

Iron chelators appear to activate the DELE1-HRI pathway in a mechanism distinct from how HRI is activated during mitochondrial stress caused by CCCP. Indeed, unlike CCCP,

neither DFO nor DFP induced mitochondrial depolarization (Figure 5A). OMA1 is a stress-responsive protease whose proteolytic activity is enhanced by mitochondrial stress-inducing agents including CCCP [45,46]. Stress-dependent OMA1 activation occurs through self-cleavage that eventually leads to the degradation of OMA1 [36,47]. Consistent with the absence of mitochondrial depolarization (Figure 5A), iron chelators appeared not to induce OMA1 activation, which was monitored by the processing of OMA1 itself, as well as its known substrates OPA1 and PGAM5 [45,46,48,49] (Figure 5B). Moreover, knockdown of OMA1 did not suppress iron chelation-induced ISR activation in HEK293T or HeLa cells (Figures 5C and 5D), indicating that OMA1 is not required for iron-deficiency-induced HRI activation.

Our immunoprecipitation assay revealed that the increase in DELE1 upon iron chelation coincided with more HRI binding to DELE1 (Figure 5E). We examined the subcellular localization of the iron deficiency-induced interaction between HRI and DELE1 using a proximity ligation assay (PLA) (Figures 5F and S4A). We observed robust increases in PLA signals after DFO, DFP, or CCCP treatment (Figure S4A). In contrast, no PLA signals were observed without expression of DELE1 (Figure S4A). These results indicate that PLA signals were derived from the stimuli-dependent interaction between HRI and DELE1. Strikingly, in iron-deficient conditions, the PLA signal was predominantly observed on, or in close proximity to, mitochondrial strings (Figure 5F). In contrast, the PLA signal was diffusely scattered over the cytosol under CCCP-treated conditions (Figure 5F). These results suggest that DELE1 interacts with HRI predominantly on the mitochondrial surface under iron deficient conditions, while this interaction occurs mainly in the cytosol under CCCP-treated conditions.

We thus considered that the mitochondrial import arrest of DELE1 (Figures 3B–3E) resulted in retention of the C-terminal TPR domains on the mitochondrial surface, allowing for the folding of the TPR domains able to subsequently interact with and activate cytosolic HRI. To test if the cytosolic exposure of the DELE1 TPR domains on the mitochondrial surface is sufficient for HRI activation, we tethered DELE1 to the OMM by fusing DELE1(d101 or d200) with a signal sequence (SS) of the OMM-localized protein TOM20 (Figures 5G and S4B), and examined whether this fusion protein can activate the HRI-ISR pathway. Both OMM-tethered DELE1s [TOMM20(SS)-DELE1(d101) and TOMM20(SS)-DELE1(d200)] were more stable than DELE1 WT under steady state conditions (Figure S4C), which is consistent with our observation that DELE1 is degraded in the matrix (Figures 1D and 1E). Also, unlike DELE1 WT, we did not observe iron deficiency-induced stabilization of these DELE1 mutants (Figure S4C). In agreement with the ability of cytosolic full-length DELE1 to bind to HRI and trigger the ISR [27], expression of the OMM-tethered DELE1 alone induced ATF4 expression without iron chelation (Figure 5G). Furthermore, knockdown of HRI abrogated this ATF4 induction (Figure 5H). These results indicate that the OMM-tethered DELE1 can act as a constitutively active form for ISR induction, supporting our hypothesis that in iron deficiency, the exposure of the DELE1 TPR domains on the OMM is sufficient to trigger the HRI-ISR pathway.

Determination of critical factors that are required for the iron deficiency-induced ISR activation

We next sought to identify critical domains in DELE1 that are required for the iron deficiency-induced DELE1 import arrest and subsequent HRI-ISR activation. Recent data reveal that an α-helix located between 80–106 amino acids (a.a.) (Figure 6A) hampers the efficient translocation of DELE1 into the matrix, and thus promotes its OMA1-mediated cleavage in the IMS under certain settings of mitochondrial stress [27]. A DELE1 mutant that lacks these amino acids, DELE1(d80-106), stabilized after iron deficiency and rescued DFO-induced ISR activation in DELE1 KO cells (Figure S5A), suggesting that this region is dispensable for the iron-deficient DELE1 response. We also created several other DELE1 mutants including a mutant whose MTS was substituted with PINK1's MTS, PINK1(MTS)-DELE1(d101), and deletion mutants lacking the intermediate region between the DELE1 MTS and TPR domains, DELE1(d102-200) and DELE1(d200-220), or lacking the entire TPR domains, DELE1(dTPR1-7) (Figure S5B). Unexpectedly, all these DELE1 mutants were able to accumulate in response to iron deficiency (Figures S5C and S5D), suggesting that iron deficiency-induced DELE1 stabilization may not be solely regulated through a single domain or motif in DELE1. Nevertheless, we identified DELE1(d102-200) as a unique mutant that did not rescue the iron deficiency-induced ISR activation (Figure 6B). DELE1 (d102-200) localized in mitochondria before and after iron chelation (Figure S5E). Unlike other DELE1 mutants lacking TPR domains, DELE1(d102-200) did not lose its ability to bind HRI when expressed in the cytosol following deletion of the MTS (Figure 6C). However, DELE1(d102-200) lost the ability to interact with HRI in a DFO-dependent manner (Figure 6D). These observations suggest that the TPR domains in this mutant may not be fully exposed into the cytosol under iron deficient conditions. The 102–200 region of DELE1 does not have any known domains or motifs except for the reported OMA1 cleavage site [17], and the latter half of this region is predicted to be disordered (Figure 6A). We thus speculated that the length of this intermediate region between the MTS and TPR domains might be important for DELE1 passing through the IMS and the OMM and fully exposing the TPR domains to the cytosol when DELE1's import is arrested (Figure 6G). Consistent with this notion, 50 a.a. deletion either in the first half or the latter half of the 102–200 a.a. [DELE1(d102-150) or DELE1(d150-200)] was able to rescue iron deficiency-induced ISR activation in DELE1 KO cells (Figure 6E). Furthermore, replacement of the 102–200 region of DELE1 with different length of amino acid linkers (20, 50, and 100 a.a.) derived from an intrinsically disordered region of Nucleolin (Figure S5F) [50] demonstrated that a length of more than 50 a.a. within this region was sufficient for this response (Figure 6F). These results support our notion that in the setting of iron deficiency, DELE1 import arrest enables the protein to cytosolically expose its TPR domains, thereby facilitating interaction with HRI on the mitochondrial surface (Figure 6G).

Next, we tried to identify external factors that are involved in the iron deficiency-induced ISR activation. Recent studies have revealed that LONP1 physically and functionally associates with mitochondrial import machineries [51,52]. Thus, we examined the possibility that LONP1 is involved in the iron deficiency-induced ISR activation through regulating the DELE1 import status. However, we did not see any defects in iron deficiency-induced ISR activation following LONP1 knockdown (Figure S6A). As previously reported [16], the

LONP1 knockdown slightly activated the ISR at steady state (Figure S6A), which may imply the presence of mitochondrial proteotoxic stress in LONP1-deficient cells, as LONP1 is a key quality control protease [30].

It has been suggested that the mitochondrial stress-activated ISR in mammalian cells is a functional counterpart of mtUPR in *C. elegans* [14,53,54] that is activated by mitochondrial proteotoxic stress-induced mitochondrial import arrest of the transcription factor ATFS-1 [25,55]. HAF-1, the IMM-resident ATP-binding cassette (ABC) transporter, was identified as a critical factor for the mitochondrial import arrest of ATFS-1 [55,56]. In mammals, there are three IMM-resident ABC transporters (ABCB7, ABCB8 and ABCB10) [57,58]. To date, the exact substrates of these transporters have not been fully determined, but, intriguingly, all of these transporters are reported to play critical roles in the intracellular and mitochondrial metabolism of iron-containing cofactors including ISC and heme [59–65]. We thus examined whether these IMM ABC transporters are also involved in the iron depletion-induced ISR activation. Knockdown of ABCB7 or ABCB8, but not ABCB10, attenuated iron deficiency-induced ATF4 expression (Figure 6H). Because ABCB8 knockdown severely impaired cell growth, we focused our subsequent efforts on ABCB7. Notably, ABCB7 was selectively required for the ISR activation by iron chelators DFO and DFP but not for that induced by CCCP (Figure 6I and 6J). Furthermore, CHX-chase experiments revealed that stabilization of DELE1 in response to iron chelation was less efficient in ABCB7 knockdown cells (Figures 6K and 6L). Moreover, similar results were obtained by the ablation of ISCU [66], a matrix-resident essential scaffold component of the ISC assembly (Figures S6B and S6C). As previously reported [65,67], we observed retardation of mitochondrial and/or cytosolic ISC biosynthesis after 72 hours of siRNA treatments for *ABCB7* or *ISCU* as evident by decreases in mitochondrial and/or cytosolic ISC-containing proteins (Figure S6D). These results suggest that with iron deficiency, a potential cross-talk may exist between ISC biosynthesis and the DELE1-HRI-ISR pathway, presumably through modulating the mitochondrial DELE1 import status.

DELE1-HRI-ISR pathway protects erythroid cells against iron deficiency-induced cell death

Lastly, to address the physiological significance of this iron-deficiency-activated DELE1-HRI pathway, we focused on erythroid cells. These cells incorporate large amounts of iron for hemoglobin synthesis, and therefore require tight regulation of intracellular iron homeostasis [68]. We employed murine erythroleukemia (MEL) cells as a well-established *in vitro* model of erythroid differentiation, and generated *DELE1* or *HRI* gene-deleted MEL cells using CRISPR (Figure S7A). Culturing MEL cells with medium containing 2% DMSO rapidly induces erythroid-like differentiation, as evident by elevated expression of erythroid marker genes within 24 hours [69]. It has been previously demonstrated that iron limitation by DFO significantly suppresses erythroid differentiation of MEL cells [69]. We found that DFO treatment during the initial 24 hours of DMSO-stimulated differentiation increased ATF4 expression, suggesting that iron-deficiency activates the ISR in differentiating MEL cells (Figure 7A). This DFO-induced ATF4 expression was markedly suppressed in DELE1 KO as well as HRI KO MEL cells when compared with WT cells (Figures 7A and 7B). Exogenous expression of DELE1 recovered ATF4 induction in iron-deficient DELE1 KO MEL cells (Figure 7C). Furthermore, RNA sequencing analyses using these MEL cell lines

revealed that upregulation of ISR target genes (such as *ATF4, DDIT3*, *TRIB3*, *MTHFD2*, and *SLC3A2*) by iron chelation was significantly attenuated in both DELE1 KO and HRI KO cells (Figures 7D and 7E and Table S1). This indicates that the DELE1-HRI pathway is required for iron-deficiency-induced ISR activation in differentiating MEL cells. Moreover, we found that DELE1 KO and HRI KO cells exhibited higher cell death following 48 hours of DFO treatment (Figure 7F). Collectively, these findings suggest that the DELE1-HRI mediated ISR plays a crucial role in protecting erythroid cells from cell death following a perturbation of iron homeostasis.

Discussion

Based on these findings, we propose a following model of DELE1-mediated HRI activation under low iron conditions (Figure 7G). Under steady state conditions where enough iron is available, DELE1 is constitutively degraded by the matrix-resident protease LONP1 soon after mitochondrial import, thereby maintaining low steady-state levels of DELE1 expression (Figure 7G, left). When intracellular iron availability is limited, the mitochondrial import of DELE1 is arrested (Figure 7G, right, step 1). This iron deficiency-induced mitochondrial import arrest of DELE1 enables DELE1 to escape from LONP1-mediated degradation (Figure 7G, right, step 2). As a consequence, full-length DELE1 is stabilized at mitochondria with its C-terminal domain exposed to the cytosol, and thereby allowing the TPR domains to fold and interact with HRI (Figure 7G, right, step 3). The stabilized, full-length form of DELE1 passes through the IMS and the OMM through an unknown mechanism. Importantly, the iron deficiency-induced activation of DELE1-HRI-ISR pathway does not require OMA1-mediated DELE1 cleavage (Figures 5C and 5D). Recent work uncovered that mitochondrial import stress (e.g., knockdown of mitochondrial import machineries or overexpression of mitochondrial precursor proteins) activates DELE1-HRI-ISR pathway [27]. Of note, ISR activation in this context also does not require OMA1, and it can be mediated by full-length DELE1 that accumulates in the cytosol. Therefore, DELE1 appears to activate the HRI-ISR pathway without OMA1-mediated cleavage under certain conditions when its C-terminal TPR domain has physical access to cytosolic HRI.

Recent studies have revealed the importance of mitochondrial import regulation in sensing various mitochondrial perturbations and triggering appropriate stress responses, as represented by the PINK1/Parkin-mediated mitophagy triggered by PINK1 import arrest [22] and the mtUPR in *C. elegans* triggered by ATFS-1 import arrest [25]. Notably, expression of both proteins is kept at a low level in the absence of stress by constitutive degradation. In both cases, the stress-dependent import arrest enables them to escape from this degradation to elicit a stress response. The constitutive degradation of these proteins appears to be an energy-consuming process but allows a rapid response to stress sensed within mitochondria. Similar to PINK1 and ATFS-1, DELE1 import arrest underscores this general mechanism of mitochondrial stress sensing, in this case to sensing intracellular iron deficiency to activate the ISR. Particularly, our findings demonstrated the mechanistic similarity between the ATFS-1-dependent mtUPR and the DELE1-dependent ISR: namely, the requirement of LONP1 for steady state degradation of the stress sensor and ABC transporters for the stress-dependent activation.

Similar to ATFS-1, a previous report suggests that the DELE1-HRI-ISR pathway is activated by mitochondrial proteotoxic stress. LONP1 deletion or mitochondrial chaperone inhibitor-mediated ISR activation was shown to be dependent on DELE1 [16]. It is noteworthy that iron chelation may also cause mitochondrial proteotoxic stress. Under iron-limited conditions, the biosynthesis of ISC is impaired, generating unfolded or misfolded ISC proteins in the mitochondrial matrix, which can become substrates for LONP1 (Figure S2A) [35]. Therefore, the accumulation of misfolded ISC proteins by iron deficiency may increase the substrate burden on LONP1, thereby decreasing the ability of LONP1 to degrade DELE1. This could be an alternative explanation for how iron deficiency-induces DELE1 stabilization. Although we do not exclude this possibility, our results support the notion that iron chelation-induced DELE1 stabilization does not solely result from the loss of LONP1 function. First, LONP1 knockdown and iron chelation stabilize different species of DELE1 (Figure 3E). LONP1 knockdown stabilized both the full-length and the MPP-cleaved form of DELE1 while iron chelation predominantly stabilized the full-length form. Therefore, iron deficiency prevents DELE1 to reach the mitochondrial matrix regardless of the LONP1 activity status. Second, although LONP1 knockdown cells exhibited slightly higher ATF4 levels at steady state, we still observed iron chelator-dependent induction of ATF4 in these cells (Figure S6A). These observations indicate the existence of an additional layer of regulation, namely the DELE1 import regulation, leading to more robust activation of ISR under iron deficient conditions, compared to LONP1 inactivation alone.

There are few examples of proteins whose mitochondrial import is regulated by iron. In our study, iron deficiency-dependent import arrest was observed only for DELE1, but not for two other MTS-containing proteins we tested (Figures 3G and 3H). A recent report identified that FTMT, a mitochondrial ferritin, may also be subject to import arrest in iron deficiency, and that this regulation may be related to its role in iron depletion-induced mitophagy [32]. It has been demonstrated that ATFS-1 is activated by *P. aeruginosa* infection, in addition to the mitochondrial proteotoxic stress [70]. Intriguingly, the exposure of worms to *P. aeruginosa* strains lacking siderophore, a bacterial toxic compound that has an iron-chelating activity, resulted in less mtUPR activation than that induced by wild-type *P. aeruginosa* [70]. Thus, it is tempting to speculate that ATFS-1 import might also be sensitive to bacterial toxin-mediated iron chelation, and possibly to other iron-deficient conditions.

We observed that the ablation of ABCB7 and ISCU, components involved in ISC metabolism, attenuated iron deficiency-induced ISR activation and DELE1 stabilization (Figures 6I–6L and S6B–S6C). Given lack of ABCB7 and ISCU impaired the maturation of mitochondrial ISC-containing proteins (Figure S6D), it is tempting to speculate that their common target, mitochondrial ISC, regulates the import of DELE1. However, as intracellular iron-cofactor metabolism pathways are highly interconnected, several alternative mechanisms are possible. Loss-of-function mutations in ABCB7 cause X-linked sideroblastic anemia with ataxia, highlighting its importance in erythrocyte maturation [64]. Consistently, ABCB7 was also reported to be involved in heme biosynthesis through its interaction with ABCB10 and FECH, two critical components in heme metabolism [65]. However, the contribution of heme in DELE1 import regulation may not be significant, as the effect of hemin on iron deficiency-induced DELE1 stabilization was modest (Figure 4F) and knockdown of ABCB10 did not suppress ISR activation by DFO (Figure 6H).

Alternatively, it is possible that perturbed intracellular and/or mitochondrial iron metabolism in ABCB7- or ISCU-deficient cells may affect the DELE1 stability. It has been reported that the ablation of ABCB7 (and ABCB8) results in mitochondrial iron overload [59,65,71]. The ablation of ISCU also affects the intracellular iron metabolism [67]. Nevertheless, either scenario supports our conclusion that DELE1 responds to changes in intracellular iron availability.

A pro-survival role for the HRI-ISR pathway in erythroid cells has been well established [12]. Analysis of HRI KO mice fed an iron-deficient diet has indicated that the HRI-mediated ISR suppresses translation of globin in order to prevent toxic aggregation of heme-deficient globin under heme-limited conditions caused by iron deficiency, thereby protecting erythroid progenitors. By using DMSO-stimulated MEL cells as an erythroid cell model, we also indicated a cell protective role for the DELE1-HRI-ISR pathway in the setting of iron deficiency (Figure 7F). It has been reported that the DELE1-HRI-ISR pathway also act as a cell death promoter in some contexts. For example, the deletion of DELE1 or HRI prevented cell death under mitochondrial stress induced by CCCP [16]. We observed DFO-induced ISR activation was relatively weak and slow compared to the CCCP-induced ISR (Figure 4A). We also showed different subcellular localizations of the DELE1-HRI interaction between iron chelation (mitochondrial surface) and CCCP (the cytosol) (Figure 5F). Thus, temporal and spatial regulation of this pathway might be important for determining cellular outcomes under various stress conditions.

The iron-dependent mitochondrial import regulation of DELE1 and its critical role in the activation of HRI we described in this study represent a previously unrecognized mitochondrial-based iron sensing mechanism connecting mitochondria to the cytosolic ISR. Mitochondria are the major iron containing subcellular compartment, as they harbor the biosynthetic pathways for two major iron cofactors, heme and ISC. Therefore, it is not surprising that mitochondria would have their own iron monitoring system, in addition to the well-characterized iron homeostasis mechanism governed by cytosolic IRP1/2 [33].

Limitations of the study

Due to technical difficulties of compartment specific iron depletion, it has not been determined whether mitochondrial or cytoplasmic iron deficiency alone is sufficient to cause DELE1 import arrest. Our attempts using DELE1 deletion and chimera mutants indicated the complexity of the mechanism of DELE1 import arrest. To further delineate this mechanism, identification of DELE1 interacting molecules as well as targets of iron or other iron-containing small molecules during this process will be required. Although we demonstrated that iron chelators predominantly stabilized the DELE1 full-length form, we also observed accumulation of a small fraction of a DELE1 short-form, which had a similar molecular size to the OMA1-cleaved form (Figure 2A), but was generated in an apparent OMA1-independent manner (Figure 5C). As this DELE1 short-form was released into the cytosol (Figure S2B), we cannot rule out the partial contribution of this form to iron deficiency-induced ISR activation.

STAR Methods

Resource availability

Lead Contact—Further information and requests for reagents will be fulfilled by Lead Contact Shiori Sekine (sekine@pitt.edu).

Materials availability—All constructs or cell lines generated in this study are available from the lead contact upon request and completion of a Material Transfer Agreement.

Data and code availability—All RNA seq data have been deposited at SRA under the accession number PRJNA970328. Raw images were deposited to Mendeley Data (DOI: 10.17632/7p8w52928v.1). All data are publicly available as of the date of publication. Accession numbers and DOI are listed in the key resources table.

This paper does not report original code.

Any additional information required to reanalyze the data reported in this paper is available from the lead contact upon request.

Experimental Model and Subject Details: HEK293T and HeLa cells were cultured in DMEM (Gibco) supplemented with 10% FBS (VWR Life Science), 10 mM HEPES (Gibco), 1 mM Sodium pyruvate (Gibco), non-essential amino acids (Gibco) and GlutaMAX (Gibco). MEL cells (F4N, Sigma) were cultured in RPMI Medium 1640 with L-Glutamine and 25 mM HEPES (Gibco) supplemented with 10% FBS and 1 x Penicillin Streptomycin Solution (Corning). MEL cell differentiation was induced by using this RPMI medium with 2% Dimethyl sulfoxide (DMSO) (Santa Cruz).

Method Details

Transfection and reagents—For RNA interference, 20 nM Stealth siRNAs (Thermo Fisher Scientific) or 5 nM Silencer select siRNAs were transfected using Lipofectamine RNAi max transfection reagent (Thermo Fisher Scientific) during cell seeding. For transient transfection of plasmids, X-tremeGENE 9 DNA Transfection Reagent (Sigma-Aldrich) was used according to the manufacturer's protocol. All the siRNAs and reagents used in this study are listed in Table S2. Following concentration was used for each drug unless otherwise indicated in the figures: 10 μg/ml cycloheximide; 10 μM MG132; 200 nM Bafilomycin A1 (Baf. A1); 1 mM Deferoxamine (DFO); 1 mM Deferiprone (DFP); 10 μM CCCP (for HEK293T); 20 μM CCCP (for HeLa); 20 μM Hemin; 1 mM succinyl acetone (SA); 1 μg/ml Doxycycline; 20 nM TMRM.

Plasmids—All plasmids construction was performed by PCR amplification (CloneAmp HiFi PCR Premix) using the appropriate primers followed by In-Fusion HD Cloning system (Takara) into the EcoRI site of the pLVX-puro vector (Clontech) or into the BamHI/NotI site of the pRetroX-Tight-puro vector (Clontech). The original vector of the C-terminally HA-tagged Su9-TEV protease was gifted from Dr. Thomas Langer [36], and sub-cloned into the HindIII-XhoI site of pcDNA3.1 (+) [72]. The mammalian Tag (−) PINK1 expression vector was gifted from Dr. Noriyuki Matsuda [73]. For subcloning of TOM20 (SS)-DELE1

(d101)-HA or TOM20 (SS)-DELE1 (d200)-HA into pLVX-puro vector, the N-terminal 90 bp of *human TOMM20* and linker sequence 5'- ggtggatctggaggttctggtgga -3' were inserted before the DELE1 (d101) or DELE1 (d200)-coding sequence, respectively. For subcloning of PINK1 (MTS)-DELE1 (d101)-HA into pLVX-puro vector, the N-terminal 102 bp of *human PINK1* were inserted before the DELE1 (d101)-coding sequence. For replacing the 102–200 region of DELE1 with different length of linkers derived from nucleolin, the nucleotide sequences of human nucleolin coding from V46 to S65 (20 a.a.), to K95 (50 a.a.), or to S145 (100 a.a.) were PCR amplified using the NCL-GFP plasmid [74] as a template, and were inserted into pLVX-puro vector together with the PCR fragments covering DELE1 N-terminal (1–101 a.a.) or C-terminal (201–515 a.a.) regions by In-Fusion assembly. All the plasmids used in this study are listed in key resources table.

Generation of cell lines—The generation of the endogenously HA-tagged DELE1 expressing HEK293T cells was described previously [16]. To generate stably transfected cell lines, lentiviruses (for plasmids within pLVX-puro vectors) and retroviruses (for plasmids within pRetroX-Tight-puro vector) were packaged in HEK293T cells. HeLa cells were transduced with viruses with 10 μg/ml polybrene (Sigma) then optimized for protein expression via antibiotics selection. For generating the Tet-on DELE1-HA stable HeLa cell line [75] and the Tet-on Su9-DHFR-3xFlag stable HeLa cell line [72], Retro-X-Tet-on Inducible Expression System (Clontech) was used according to the manufacturer's instruction. For generating the Tet-on DELE1-HA / Mito-BFP stable HeLa cell line, Tet-on DELE1-HA stable cells were transduced with a previously reported lentiviral Mito-BFP (Addgene plasmid #49151) [76]. For generating the ATF4 reporter cell line (ATF4_uORF_mApple-stable HeLa cells), HeLa cells were transduced with a previously reported lentiviral ISR reporter pXG237 containing two ATF4 upstream open reading frames upstream of mApple [17] (Addgene plasmid #141281). A clonal cell line was produced by single-cell sorting into a 96-well plate. For generating the DELE1 KO HEK293T cell lines, the lentiCRISPRv2 system [77–79] was used. Two sgRNAs were designed to target the 5' and 3' intron region of Exon2 of the *DELE1* gene as shown in Figure S1; 5' intron region (5'-ggagaccagcagaatcacat-3') and 3' intron region (5'-ctcatttcctcccctagtca-3'). After the infection of lentiviruses that express hSpCas9 and DELE1 sgRNAs, infected cells were selected via the treatment with 500 μg/ml puromycin (Sigma) for 24 hours. The selected cells were subjected to single colony isolation in 96-well plates. Genomic DNA of the DELE1 KO clones (#24 and #51) used in this study were extracted with the Genotyping Buffer [100 mM Tris-HCl pH 8.0, 5 mM EDTA, 200 mM NaCl, 0.1% SDS, 0.2 mg/ml proteinase K (Thermo Fisher Scientific)] and PCR amplified using a pair of primers (forward, 5'-gtccaatggcaggagatggt-3'; reverse, 5'-aggctatcaagtaggggcaaag-3') to confirm the deletion. For generating DELE1 KO and HRI KO MEL cell lines, similar strategies were used with sgRNAs; DELE1 guide #1 (5'-TGAGACCCATCTGAACTGGT-3'), DELE1 guide #2 (5'-CAGGTTCCCACGGTTCAAAG-3'), HRI guide #1 (5'-CTGTCTCACCATCATACTTG-3'), and HRI guide #2 (5'-ATTTAAACACCTGTTTGGAG-3'). All the cell lines used in this study are described in key resources table.

Immunoblotting (IB)—The procedure for IB was previously described [75]. Cells were lysed with 1× NuPAGE LDS sample Buffer (Thermo Fisher Scientific) supplemented with 10 mM Dithiothreitol (DTT) (Sigma), and boiled at 98 °C in the bench-top thermal mixer shaking at 1,300 rpm for 15 min. Approximately, 30 – 50 μg of protein per samples were separated on an SDS-PAGE (either 7.5 %, 10 %, or 4–20% gradient) Mini-PROTEAN TGX Precast Gel (Bio-Rad) or Criterion TGX Gel (Bio-Rad) and then transferred to a nitrocellulose membrane (Bio-Rad) or a PVDF membrane (Bio-Rad). The membrane was blocked with Odyssey Blocking Buffer (LI-COR) and incubated with the indicated primary antibodies at 4°C overnight. After washing with PBS-T (PBS + 0.05% Tween-20), the membrane was incubated with HRP-conjugated secondary antibodies (Thermo Fisher Scientific) and washed again with PBS-T. Detection was performed with ECL substrates (Thermo Fisher Scientific) and iBright CL1000 Imaging System (Thermo Fisher Scientific). All the antibodies used in this study are described in key resources table.

Immunocytochemistry (ICC)—ICC was performed as previously described [75]. Cells were seeded into Lab-Tek Chambered Coverglass with 4 wells (Thermo Fisher Scientific). Cells were rinsed with PBS and fixed with PBS containing 4% formaldehyde (Thermo Fisher Scientific) for 15 min at room temperature. Cells were permeabilized with PBS containing 0.1% Triton X-100 for 10 min at room temperature. Blocking was performed using PBS containing 2% BSA (2%BSA/PBS) for 30–60 min at room temperature. For immunostaining, cells were incubated with the indicated primary antibodies, diluted in 2%BSA/PBS, overnight at 4C° and with secondary antibodies (Alexa Fluor, Thermo Fisher Scientific), diluted in 2%BSA/PBS, for about 2 hours at room temperature. Cells were imaged using a 63 × /1.4 NA oil immersion objective on Leica SP8 LIGHTNING Confocal Microscope (Leica). All the antibodies used in this study are described in key resources table.

Immunoprecipitation (IP)—For immunoprecipitation, cells were lysed with 1% Triton Buffer [1% Triton-X100, 150 mM NaCl, 50 mM Tris-HCl (pH 7.4), 1 mM EDTA, and protease inhibitors (cOmplete, Sigma)]. After centrifugation, the lysate was incubated with anti-HA Magnetic beads (Pierce) for 20 min at 4C°. After washing the beads with 1% Triton Buffer 4 times, immunoprecipitants were eluted from the beads by boiling for 3 min with 1× NuPAGE LDS sample Buffer (Thermo Fisher Scientific) supplemented with 10 mM Dithiothreitol (DTT) (Sigma) for 3 min. The samples were subjected to the immunoblotting analysis. For DSP cross-linking IP, cells were incubated with 0.1 mM DSP (Thermo Fisher Scientific)-containing ice-cold PBS for 30 min at 4C°. After removing the DSP solution, the cross-linking reaction was stopped by adding 20 mM Tris-HCl (pH 7.4) for 15 min at 4C°. After washing cells with ice-cold PBS for 3 times, cells were lysed with IP lysis buffer [20 mM Tris-HCl pH7.5, 150 mM NaCl, 10 mM EDTA pH8.0, 1% Na-DOC, 1% Triton X-100, and protease inhibitors (cOmplete, Sigma)], and were subjected to immunoprecipitation assay described above.

RNA Isolation and quantitative PCR (qPCR)—Procedures for RNA isolation and subsequent qPCR were described previously [75]. All expression levels were normalized to that of RPS18 mRNA. The following qPCR primers were used; *RPS18*, (forward)

5’-cttccacaggaggcctacac-3’ and (reverse) 5’-cgcaaaatatgctggaacttt-3’; *DELE1*, (forward) 5’-cccactggaaaggagtgttg-3’ and (reverse) 5’-acccacaggctccctctt-3’; *ABCB7*, (forward) 5’-ccacacagacccaaaagaag-3’ and (reverse) 5’-caccacccaaaaatcccag-3’; *DDIT3*, (forward) 5’-TCTTGACCCTGCTTCTCTG-3’ and (reverse) 5’-TCTTCCTCCTCTTCCTCCTG-3’; *ASNS*, (forward) 5’-GAAGAACACAGATAGCGTGG-3’ and (reverse) 5’-GGCAGAGACAAGTAATAGGAAG-3’; *CTH*, (forward) 5’-TTCCTGCCACACTTCCAAC-3’ and (reverse) 5’-TGCTGCCACTGCTTTTTC-3’; *CHAC1*, (forward) 5’-GAGGGATAGTAGGGCATGAG-3’ and (reverse) 5’-CAGACAGACAGAGGGACAAG-3’.

Flow cytometry—To determine mitochondrial membrane potential, 20 nM TMRM (Thermo Fisher Scientific) was directly added to cell culture media and incubated for 15 min. Cells were washed and replaced with normal medium followed by flow cytometry analysis using Attune N×T Acoustic Focusing Cytometer (Thermo Fisher Scientific). To determine cell viability, Propidium iodide (Thermo Fisher Scientific) was added to cell culture media and incubated for 15 min, followed by flow cytometry analysis. For the flow cytometry analysis of the ATF4 reporter cell line (ATF4_uORF_mApple-stable HeLa cells), mApple was measured on an Amnis CellStream flow cytometer (Luminex), using a 561 nm laser for excitation and a 611/31 bandwidth filter for emission. Data was analyzed from the fcs files using a custom Python 3 script and the FlowCytometryTools library.

Crude mitochondrial isolation and protease protection assay—HEK293T were treated with 10 μg/mL cycloheximide (CHX, Sigma-Aldrich, C4859) for 30 min after pre-treatment with 1 mM deferoxamine (DFO, Cayman Chemicals, 14595) or H_2O for 16 hours. HEK293T cells were scraped from cell culture plates and resuspended in cold homogenization buffer (220 mM mannitol, 70 mM sucrose, 20 mM HEPES/KOH pH 7.4, 1 mM EDTA). Mitochondria were isolated using a syringe (25G × 5/8””/ ø 0.50 × 16 mm, B. Braun, 4657853) and differential centrifugation: to remove nuclei and intact cells, two centrifugation steps at 700 × g for 10 min and 5 min at 4 °C were performed. The supernatant was then centrifuged at 8000 × g for 15 min at 4 °C. The mitochondrial pellet was resuspended in SEM Buffer and protein concentration was determined by Bradford Assay. For proteinase K digestion, 50 μg mitochondria per reaction were used. After an additional centrifugation step at 8000 × g for 10 min at 4 °C, the mitochondria were resuspended in SEM Buffer (10 mM MOPS-Tris pH 7.2, 250 mM sucrose, 1 mM EDTA), EM buffer (10 mM MOPS-Tris pH 7.2, 1 mM EDTA), or SEM buffer + 0.5% TritonX-100 and incubated on ice for 10 min. For digestion, Proteinase K (50 μg/mL; Sigma-Aldrich, P6556) was added and incubated for 10 min on ice. To stop the reaction, 1 mM final concentration phenylmethansulfonylfluorid (PMSF, Sigma-Aldrich, P7626) was added. After 15 min final incubation, SDS sample buffer was added, and samples were boiled at 95 °C for 10 min.

Proximity Ligation Assay (PLA)—PLA was performed by using Duolink In Situ PLA Probe Starter Kit (DUO92101, Sigma) according to the manufacturer’s instruction and the previously described method [80]. For PLA, cells were grown on cover glasses (CAROLINA, 633029). Cells were fixed, permeabilized, and blocked with 0.2% BSA in PBS for 1 hour at

room temperature (RT), and then incubated with the following primary antibodies overnight at 4C°; anti-HRI rabbit antibody (Proteintech, 20499–1-AP) and anti-HA mouse antibody (Cell Signaling, 2367). After washing with PBS, samples were incubated with PLA probes (DUO92101, Sigma) for 1 hour at 37C°. After washing with buffer A [0.01 M Tris-HCl (pH 7.4), 0.15 M NaCl, 0.05% Tween 20], samples were incubated with ligation mix (DUO92101, Sigma) for 30 min at 37C°. After washing with buffer A, samples were incubated with polymerase mix (DUO92101, Sigma) for 100 min at 37C°. After sequential washing by buffer B [0.2 M Tris-HCl (pH 7.4), 0.1 M NaCl] and buffer C (10 times dilution of buffer B with water), cover glasses were mounted with ProLong Gold Antifade Mountant (Invitrogen, P36934) onto a glass microscopic slide (VWR, 48311–703). Cells were imaged using a 63 × /1.4 NA oil immersion objective on Leica SP8 LIGHTNING Confocal Microscope (Leica).

RNA-sequencing—Total RNAs were isolated using RNeasy Mini Kit (Qiagen) and reverse-transcribed to cDNA using iScript cDNA Synthesis Kit (Bio-Rad) according to the manufacturer's instruction. RNA sequencing and the data analysis were performed through the commercial service provided by MedGenome, Inc (Foster City, USA). Illumina TruSeq stranded mRNA kit was used to prepare libraries according to the manufacturer's instructions. The resulting libraries were sequenced on NovaSeq 6000 using paired-end 100 base pair sequencing at the depth of 40M reads per sample.

Quantification and Statistical Analysis

Statistical significances were determined using Prism software (GraphPad Software, Inc.) as indicated in the Figure legends.

Supplementary Material

Refer to Web version on PubMed Central for supplementary material.

Acknowledgements

We thank Dr. Toren Finkel for critical reading of our manuscript, and Dr. Richard J Youle for sharing reagents. We thank Dr. Mo Chen for technical advice on PLA and Dr. Bill Chen for sharing reagents. This work was supported by University of Pittsburgh, Aging Institute Seed (S.S. and Y.S.) and a grant from NIH, NIDDK (R01DK134341, S.S. and Y.S.), as well as the NINDS intramural program (D.P.N.) and grants from the European Research Council (ERC-STG 804182 SOLID, L.T.J.) and German Research Foundation (DFG project JA 2873/2, L.T.J.).

Reference

1. Costa-Mattioli M, and Walter P (2020). The integrated stress response: From mechanism to disease. Science 368. 10.1126/science.aat5314.
2. Pakos-Zebrucka K, Koryga I, Mnich K, Ljujic M, Samali A, and Gorman AM (2016). The integrated stress response. EMBO Rep 17, 1374–1395. 10.15252/embr.201642195. [PubMed: 27629041]
3. Chen JJ, and Zhang S (2019). Heme-regulated eIF2alpha kinase in erythropoiesis and hemoglobinopathies. Blood 134, 1697–1707. 10.1182/blood.2019001915. [PubMed: 31554636]
4. Bruns GP, and London IM (1965). The Effect of Hemin on the Synthesis of Globin. Biochem Biophys Res Commun 18, 236–242. 10.1016/0006-291x(65)90746-1. [PubMed: 14282023]

5. Ranu RS, Levin DH, Delaunay J, Ernst V, and London IM (1976). Regulation of protein synthesis in rabbit reticulocyte lysates: characteristics of inhibition of protein synthesis by a translational inhibitor from heme-deficient lysates and its relationship to the initiation factor which binds Met-tRNAf. Proc Natl Acad Sci U S A 73, 2720–2724. 10.1073/pnas.73.8.2720. [PubMed: 1066685]
6. Ranu RS, and London IM (1976). Regulation of protein synthesis in rabbit reticulocyte lysates: purification and initial characterization of the cyclic 3':5'-AMP independent protein kinase of the heme-regulated translational inhibitor. Proc Natl Acad Sci U S A 73, 4349–4353. 10.1073/pnas.73.12.4349. [PubMed: 1069987]
7. Trachsel H, Ranu RS, and London IM (1978). Regulation of protein synthesis in rabbit reticulocyte lysates: purification and characterization of heme-reversible translational inhibitor. Proc Natl Acad Sci U S A 75, 3654–3658. 10.1073/pnas.75.8.3654. [PubMed: 278981]
8. Fagard R, and London IM (1981). Relationship between phosphorylation and activity of heme-regulated eukaryotic initiation factor 2 alpha kinase. Proc Natl Acad Sci U S A 78, 866–870. 10.1073/pnas.78.2.866. [PubMed: 6940153]
9. Rafie-Kolpin M, Chefalo PJ, Hussain Z, Hahn J, Uma S, Matts RL, and Chen JJ (2000). Two heme-binding domains of heme-regulated eukaryotic initiation factor-2alpha kinase. N terminus and kinase insertion. J Biol Chem 275, 5171–5178. 10.1074/jbc.275.7.5171. [PubMed: 10671563]
10. Igarashi J, Murase M, Iizuka A, Pichierri F, Martinkova M, and Shimizu T (2008). Elucidation of the heme binding site of heme-regulated eukaryotic initiation factor 2alpha kinase and the role of the regulatory motif in heme sensing by spectroscopic and catalytic studies of mutant proteins. J Biol Chem 283, 18782–18791. 10.1074/jbc.M801400200. [PubMed: 18450746]
11. Miksanova M, Igarashi J, Minami M, Sagami I, Yamauchi S, Kurokawa H, and Shimizu T (2006). Characterization of heme-regulated eIF2alpha kinase: roles of the N-terminal domain in the oligomeric state, heme binding, catalysis, and inhibition. Biochemistry 45, 9894–9905. 10.1021/bi060556k. [PubMed: 16893190]
12. Han AP, Yu C, Lu L, Fujiwara Y, Browne C, Chin G, Fleming M, Leboulch P, Orkin SH, and Chen JJ (2001). Heme-regulated eIF2alpha kinase (HRI) is required for translational regulation and survival of erythroid precursors in iron deficiency. EMBO J 20, 6909–6918. 10.1093/emboj/20.23.6909. [PubMed: 11726526]
13. Taniuchi S, Miyake M, Tsugawa K, Oyadomari M, and Oyadomari S (2016). Integrated stress response of vertebrates is regulated by four eIF2alpha kinases. Sci Rep 6, 32886. 10.1038/srep32886. [PubMed: 27633668]
14. Quiros PM, Prado MA, Zamboni N, D'Amico D, Williams RW, Finley D, Gygi SP, and Auwerx J (2017). Multi-omics analysis identifies ATF4 as a key regulator of the mitochondrial stress response in mammals. J Cell Biol 216, 2027–2045. 10.1083/jcb.201702058. [PubMed: 28566324]
15. Munch C, and Harper JW (2016). Mitochondrial unfolded protein response controls matrix pre-RNA processing and translation. Nature 534, 710–713. 10.1038/nature18302. [PubMed: 27350246]
16. Fessler E, Eckl EM, Schmitt S, Mancilla IA, Meyer-Bender MF, Hanf M, Philippou-Massier J, Krebs S, Zischka H, and Jae LT (2020). A pathway coordinated by DELE1 relays mitochondrial stress to the cytosol. Nature 579, 433–437. 10.1038/s41586-020-2076-4. [PubMed: 32132706]
17. Guo X, Aviles G, Liu Y, Tian R, Unger BA, Lin YT, Wiita AP, Xu K, Correia MA, and Kampmann M (2020). Mitochondrial stress is relayed to the cytosol by an OMA1-DELE1-HRI pathway. Nature 579, 427–432. 10.1038/s41586-020-2078-2. [PubMed: 32132707]
18. Ahola S, Rivera Mejias P, Hermans S, Chandragiri S, Giavalisco P, Nolte H, and Langer T (2022). OMA1-mediated integrated stress response protects against ferroptosis in mitochondrial cardiomyopathy. Cell Metab 34, 1875–1891 e1877. 10.1016/j.cmet.2022.08.017. [PubMed: 36113464]
19. Shammas MK, Huang X, Wu BP, Fessler E, Song IY, Randolph NP, Li Y, Bleck CK, Springer DA, Fratter C, et al. (2022). OMA1 mediates local and global stress responses against protein misfolding in CHCHD10 mitochondrial myopathy. J Clin Invest 132. 10.1172/JCI157504.
20. Huynh H, Zhu S, Lee S, Bao Y, Pang J, Nguyen A, Gu Y, Chen C, Ouyang K, Evans SM, and Fang X (2022). DELE1 is protective for mitochondrial cardiomyopathy. J Mol Cell Cardiol 175, 44–48. 10.1016/j.yjmcc.2022.12.003. [PubMed: 36539111]

21. Zhu S, Nguyen A, Pang J, Zhao J, Chen Z, Liang Z, Gu Y, Huynh H, Bao Y, Lee S, et al. (2022). Mitochondrial Stress Induces an HRI-eIF2alpha Pathway Protective for Cardiomyopathy. Circulation 146, 1028–1031. 10.1161/CIRCULATIONAHA.122.059594. [PubMed: 36154620]
22. Sekine S, and Youle RJ (2018). PINK1 import regulation; a fine system to convey mitochondrial stress to the cytosol. BMC Biol 16, 2. 10.1186/s12915-017-0470-7. [PubMed: 29325568]
23. Narendra DP, Jin SM, Tanaka A, Suen DF, Gautier CA, Shen J, Cookson MR, and Youle RJ (2010). PINK1 is selectively stabilized on impaired mitochondria to activate Parkin. PLoS Biol 8, e1000298. 10.1371/journal.pbio.1000298. [PubMed: 20126261]
24. Matsuda N, Sato S, Shiba K, Okatsu K, Saisho K, Gautier CA, Sou YS, Saiki S, Kawajiri S, Sato F, et al. (2010). PINK1 stabilized by mitochondrial depolarization recruits Parkin to damaged mitochondria and activates latent Parkin for mitophagy. J Cell Biol 189, 211–221. 10.1083/jcb.200910140. [PubMed: 20404107]
25. Anderson NS, and Haynes CM (2020). Folding the Mitochondrial UPR into the Integrated Stress Response. Trends Cell Biol 30, 428–439. 10.1016/j.tcb.2020.03.001. [PubMed: 32413314]
26. Harada T, Iwai A, and Miyazaki T (2010). Identification of DELE, a novel DAP3-binding protein which is crucial for death receptor-mediated apoptosis induction. Apoptosis 15, 1247–1255. 10.1007/s10495-010-0519-3. [PubMed: 20563667]
27. Fessler E, Krumwiede L, and Jae LT (2022). DELE1 tracks perturbed protein import and processing in human mitochondria. Nat Commun 13, 1853. 10.1038/s41467-022-29479-y. [PubMed: 35388015]
28. Ueno T, and Komatsu M (2020). Monitoring Autophagy Flux and Activity: Principles and Applications. Bioessays 42, e2000122. 10.1002/bies.202000122. [PubMed: 32851706]
29. Deshwal S, Fiedler KU, and Langer T (2020). Mitochondrial Proteases: Multifaceted Regulators of Mitochondrial Plasticity. Annu Rev Biochem 89, 501–528. 10.1146/annurev-biochem-062917-012739. [PubMed: 32075415]
30. Szczepanowska K, and Trifunovic A (2021). Mitochondrial matrix proteases: quality control and beyond. FEBS J. 10.1111/febs.15964.
31. Fujimaki M, Furuya N, Saiki S, Amo T, Imamichi Y, and Hattori N (2019). Iron Supply via NCOA4-Mediated Ferritin Degradation Maintains Mitochondrial Functions. Mol Cell Biol 39. 10.1128/MCB.00010-19.
32. Hara Y, Yanatori I, Tanaka A, Kishi F, Lemasters JJ, Nishina S, Sasaki K, and Hino K (2020). Iron loss triggers mitophagy through induction of mitochondrial ferritin. EMBO Rep 21, e50202. 10.15252/embr.202050202. [PubMed: 32975364]
33. Hentze MW, Muckenthaler MU, Galy B, and Camaschella C (2010). Two to tango: regulation of Mammalian iron metabolism. Cell 142, 24–38. 10.1016/j.cell.2010.06.028. [PubMed: 20603012]
34. Fukasawa Y, Tsuji J, Fu SC, Tomii K, Horton P, and Imai K (2015). MitoFates: improved prediction of mitochondrial targeting sequences and their cleavage sites. Mol Cell Proteomics 14, 1113–1126. 10.1074/mcp.M114.043083. [PubMed: 25670805]
35. Maio N, Ghezzi D, Verrigni D, Rizza T, Bertini E, Martinelli D, Zeviani M, Singh A, Carrozzo R, and Rouault TA (2016). Disease-Causing SDHAF1 Mutations Impair Transfer of Fe-S Clusters to SDHB. Cell Metab 23, 292–302. 10.1016/j.cmet.2015.12.005. [PubMed: 26749241]
36. Baker MJ, Lampe PA, Stojanovski D, Korwitz A, Anand R, Tatsuta T, and Langer T (2014). Stress-induced OMA1 activation and autocatalytic turnover regulate OPA1-dependent mitochondrial dynamics. EMBO J 33, 578–593. 10.1002/embj.201386474. [PubMed: 24550258]
37. Lazarou M, Jin SM, Kane LA, and Youle RJ (2012). Role of PINK1 binding to the TOM complex and alternate intracellular membranes in recruitment and activation of the E3 ligase Parkin. Dev Cell 22, 320–333. 10.1016/j.devcel.2011.12.014. [PubMed: 22280891]
38. Okatsu K, Uno M, Koyano F, Go E, Kimura M, Oka T, Tanaka K, and Matsuda N (2013). A dimeric PINK1-containing complex on depolarized mitochondria stimulates Parkin recruitment. J Biol Chem 288, 36372–36384. 10.1074/jbc.M113.509653. [PubMed: 24189060]
39. Akabane S, Watanabe K, Kosako H, Yamashita SI, Nishino K, Kato M, Sekine S, Kanki T, Matsuda N, Endo T, and Oka T (2023). TIM23 facilitates PINK1 activation by safeguarding against OMA1-mediated degradation in damaged mitochondria. Cell Rep, 112454. 10.1016/j.celrep.2023.112454.

40. Sekine S (2020). PINK1 import regulation at a crossroad of mitochondrial fate: the molecular mechanisms of PINK1 import. J Biochem 167, 217–224. 10.1093/jb/mvz069. [PubMed: 31504668]
41. Wiedemann N, and Pfanner N (2017). Mitochondrial Machineries for Protein Import and Assembly. Annu Rev Biochem 86, 685–714. 10.1146/annurev-biochem-060815-014352. [PubMed: 28301740]
42. Sekine Y, Zyryanova A, Crespillo-Casado A, Fischer PM, Harding HP, and Ron D (2015). Stress responses. Mutations in a translation initiation factor identify the target of a memory-enhancing compound. Science 348, 1027–1030. 10.1126/science.aaa6986. [PubMed: 25858979]
43. Sidrauski C, Acosta-Alvear D, Khoutorsky A, Vedantham P, Hearn BR, Li H, Gamache K, Gallagher CM, Ang KK, Wilson C, et al. (2013). Pharmacological brake-release of mRNA translation enhances cognitive memory. Elife 2, e00498. 10.7554/eLife.00498. [PubMed: 23741617]
44. Igarashi K, and Sun J (2006). The heme-Bach1 pathway in the regulation of oxidative stress response and erythroid differentiation. Antioxid Redox Signal 8, 107–118. 10.1089/ars.2006.8.107. [PubMed: 16487043]
45. Ehses S, Raschke I, Mancuso G, Bernacchia A, Geimer S, Tondera D, Martinou JC, Westermann B, Rugarli EI, and Langer T (2009). Regulation of OPA1 processing and mitochondrial fusion by m-AAA protease isoenzymes and OMA1. J Cell Biol 187, 1023–1036. 10.1083/jcb.200906084. [PubMed: 20038678]
46. Head B, Griparic L, Amiri M, Gandre-Babbe S, and van der Bliek AM (2009). Inducible proteolytic inactivation of OPA1 mediated by the OMA1 protease in mammalian cells. J Cell Biol 187, 959–966. 10.1083/jcb.200906083. [PubMed: 20038677]
47. Zhang K, Li H, and Song Z (2014). Membrane depolarization activates the mitochondrial protease OMA1 by stimulating self-cleavage. EMBO Rep 15, 576–585. 10.1002/embr.201338240. [PubMed: 24719224]
48. Wai T, Saita S, Nolte H, Muller S, Konig T, Richter-Dennerlein R, Sprenger HG, Madrenas J, Muhlmeister M, Brandt U, et al. (2016). The membrane scaffold SLP2 anchors a proteolytic hub in mitochondria containing PARL and the i-AAA protease YME1L. EMBO Rep 17, 1844–1856. 10.15252/embr.201642698. [PubMed: 27737933]
49. Sekine S, Kanamaru Y, Koike M, Nishihara A, Okada M, Kinoshita H, Kamiyama M, Maruyama J, Uchiyama Y, Ishihara N, et al. (2012). Rhomboid protease PARL mediates the mitochondrial membrane potential loss-induced cleavage of PGAM5. J Biol Chem 287, 34635–34645. 10.1074/jbc.M112.357509. [PubMed: 22915595]
50. Emmott E, and Hiscox JA (2009). Nucleolar targeting: the hub of the matter. EMBO Rep 10, 231–238. 10.1038/embor.2009.14. [PubMed: 19229283]
51. Shin CS, Meng S, Garbis SD, Moradian A, Taylor RW, Sweredoski MJ, Lomenick B, and Chan DC (2021). LONP1 and mtHSP70 cooperate to promote mitochondrial protein folding. Nat Commun 12, 265. 10.1038/s41467-020-20597-z. [PubMed: 33431889]
52. Matsushima Y, Takahashi K, Yue S, Fujiyoshi Y, Yoshioka H, Aihara M, Setoyama D, Uchiumi T, Fukuchi S, and Kang D (2021). Mitochondrial Lon protease is a gatekeeper for proteins newly imported into the matrix. Commun Biol 4, 974. 10.1038/s42003-021-02498-z. [PubMed: 34400774]
53. Fiorese CJ, Schulz AM, Lin YF, Rosin N, Pellegrino MW, and Haynes CM (2016). The Transcription Factor ATF5 Mediates a Mammalian Mitochondrial UPR. Curr Biol 26, 2037–2043. 10.1016/j.cub.2016.06.002. [PubMed: 27426517]
54. Eckl EM, Ziegemann O, Krumwiede L, Fessler E, and Jae LT (2021). Sensing, signaling and surviving mitochondrial stress. Cell Mol Life Sci 78, 5925–5951. 10.1007/s00018-021-03887-7. [PubMed: 34228161]
55. Nargund AM, Pellegrino MW, Fiorese CJ, Baker BM, and Haynes CM (2012). Mitochondrial import efficiency of ATFS-1 regulates mitochondrial UPR activation. Science 337, 587–590. 10.1126/science.1223560. [PubMed: 22700657]

56. Haynes CM, Yang Y, Blais SP, Neubert TA, and Ron D (2010). The matrix peptide exporter HAF-1 signals a mitochondrial UPR by activating the transcription factor ZC376.7 in C. elegans. Mol Cell 37, 529–540. 10.1016/j.molcel.2010.01.015. [PubMed: 20188671]
57. Schaedler TA, Faust B, Shintre CA, Carpenter EP, Srinivasan V, van Veen HW, and Balk J (2015). Structures and functions of mitochondrial ABC transporters. Biochem Soc Trans 43, 943–951. 10.1042/BST20150118. [PubMed: 26517908]
58. Liesa M, Qiu W, and Shirihai OS (2012). Mitochondrial ABC transporters function: the role of ABCB10 (ABC-me) as a novel player in cellular handling of reactive oxygen species. Biochim Biophys Acta 1823, 1945–1957. 10.1016/j.bbamcr.2012.07.013. [PubMed: 22884976]
59. Ichikawa Y, Bayeva M, Ghanefar M, Potini V, Sun L, Mutharasan RK, Wu R, Khechaduri A, Jairaj Naik T, and Ardehali H (2012). Disruption of ATP-binding cassette B8 in mice leads to cardiomyopathy through a decrease in mitochondrial iron export. Proc Natl Acad Sci U S A 109, 4152–4157. 10.1073/pnas.1119338109. [PubMed: 22375032]
60. Pondarre C, Antiochos BB, Campagna DR, Clarke SL, Greer EL, Deck KM, McDonald A, Han AP, Medlock A, Kutok JL, et al. (2006). The mitochondrial ATP-binding cassette transporter Abcb7 is essential in mice and participates in cytosolic iron-sulfur cluster biogenesis. Hum Mol Genet 15, 953–964. 10.1093/hmg/ddl012. [PubMed: 16467350]
61. Pondarre C, Campagna DR, Antiochos B, Sikorski L, Mulhern H, and Fleming MD (2007). Abcb7, the gene responsible for X-linked sideroblastic anemia with ataxia, is essential for hematopoiesis. Blood 109, 3567–3569. 10.1182/blood-2006-04-015768. [PubMed: 17192398]
62. Hyde BB, Liesa M, Elorza AA, Qiu W, Haigh SE, Richey L, Mikkola HK, Schlaeger TM, and Shirihai OS (2012). The mitochondrial transporter ABC-me (ABCB10), a downstream target of GATA-1, is essential for erythropoiesis in vivo. Cell Death Differ 19, 1117–1126. 10.1038/cdd.2011.195. [PubMed: 22240895]
63. Yamamoto M, Arimura H, Fukushige T, Minami K, Nishizawa Y, Tanimoto A, Kanekura T, Nakagawa M, Akiyama S, and Furukawa T (2014). Abcb10 role in heme biosynthesis in vivo: Abcb10 knockout in mice causes anemia with protoporphyrin IX and iron accumulation. Mol Cell Biol 34, 1077–1084. 10.1128/MCB.00865-13. [PubMed: 24421385]
64. Shimada Y, Okuno S, Kawai A, Shinomiya H, Saito A, Suzuki M, Omori Y, Nishino N, Kanemoto N, Fujiwara T, et al. (1998). Cloning and chromosomal mapping of a novel ABC transporter gene (hABC7), a candidate for X-linked sideroblastic anemia with spinocerebellar ataxia. J Hum Genet 43, 115–122. 10.1007/s100380050051. [PubMed: 9621516]
65. Maio N, Kim KS, Holmes-Hampton G, Singh A, and Rouault TA (2019). Dimeric ferrochelatase bridges ABCB7 and ABCB10 homodimers in an architecturally defined molecular complex required for heme biosynthesis. Haematologica 104, 1756–1767. 10.3324/haematol.2018.214320. [PubMed: 30765471]
66. Lill R, and Freibert SA (2020). Mechanisms of Mitochondrial Iron-Sulfur Protein Biogenesis. Annu Rev Biochem 89, 471–499. 10.1146/annurev-biochem-013118-111540. [PubMed: 31935115]
67. Tong WH, and Rouault TA (2006). Functions of mitochondrial ISCU and cytosolic ISCU in mammalian iron-sulfur cluster biogenesis and iron homeostasis. Cell Metab 3, 199–210. 10.1016/j.cmet.2006.02.003. [PubMed: 16517407]
68. Ganz T (2013). Systemic iron homeostasis. Physiol Rev 93, 1721–1741. 10.1152/physrev.00008.2013. [PubMed: 24137020]
69. Crooks DR, Ghosh MC, Haller RG, Tong WH, and Rouault TA (2010). Posttranslational stability of the heme biosynthetic enzyme ferrochelatase is dependent on iron availability and intact iron-sulfur cluster assembly machinery. Blood 115, 860–869. 10.1182/blood-2009-09-243105. [PubMed: 19965627]
70. Pellegrino MW, Nargund AM, Kirienko NV, Gillis R, Fiorese CJ, and Haynes CM (2014). Mitochondrial UPR-regulated innate immunity provides resistance to pathogen infection. Nature 516, 414–417. 10.1038/nature13818. [PubMed: 25274306]
71. Cavadini P, Biasiotto G, Poli M, Levi S, Verardi R, Zanella I, Derosas M, Ingrassia R, Corrado M, and Arosio P (2007). RNA silencing of the mitochondrial ABCB7 transporter in HeLa cells causes an iron-deficient phenotype with mitochondrial iron overload. Blood 109, 3552–3559. 10.1182/blood-2006-08-041632. [PubMed: 17192393]

72. Sekine S, Wang C, Sideris DP, Bunker E, Zhang Z, and Youle RJ (2019). Reciprocal Roles of Tom7 and OMA1 during Mitochondrial Import and Activation of PINK1. Mol Cell 73, 1028–1043 e1025. 10.1016/j.molcel.2019.01.002. [PubMed: 30733118]

73. Okatsu K, Oka T, Iguchi M, Imamura K, Kosako H, Tani N, Kimura M, Go E, Koyano F, Funayama M, et al. (2012). PINK1 autophosphorylation upon membrane potential dissipation is essential for Parkin recruitment to damaged mitochondria. Nat Commun 3, 1016. 10.1038/ncomms2016. [PubMed: 22910362]

74. Houston R, Sekine S, Calderon MJ, Seifuddin F, Wang G, Kawagishi H, Malide DA, Li Y, Gucek M, Pirooznia M, et al. (2020). Acetylation-mediated remodeling of the nucleolus regulates cellular acetyl-CoA responses. PLoS Biol 18, e3000981. 10.1371/journal.pbio.3000981. [PubMed: 33253182]

75. Houston R, Sekine Y, Larsen MB, Murakami K, Mullett SJ, Wendell SG, Narendra DP, Chen BB, and Sekine S (2021). Discovery of bactericides as an acute mitochondrial membrane damage inducer. Mol Biol Cell 32, ar32. 10.1091/mbc.E21-04-0191. [PubMed: 34495738]

76. Friedman JR, Lackner LL, West M, DiBenedetto JR, Nunnari J, and Voeltz GK (2011). ER tubules mark sites of mitochondrial division. Science 334, 358–362. 10.1126/science.1207385. [PubMed: 21885730]

77. Sanjana NE, Shalem O, and Zhang F (2014). Improved vectors and genome-wide libraries for CRISPR screening. Nat Methods 11, 783–784. 10.1038/nmeth.3047. [PubMed: 25075903]

78. Shalem O, Sanjana NE, Hartenian E, Shi X, Scott DA, Mikkelson T, Heckl D, Ebert BL, Root DE, Doench JG, and Zhang F (2014). Genome-scale CRISPR-Cas9 knockout screening in human cells. Science 343, 84–87. 10.1126/science.1247005. [PubMed: 24336571]

79. Stringer BW, Day BW, D'Souza RCJ, Jamieson PR, Ensbey KS, Bruce ZC, Lim YC, Goasdoue K, Offenhauser C, Akgul S, et al. (2019). A reference collection of patient-derived cell line and xenograft models of proneural, classical and mesenchymal glioblastoma. Sci Rep 9, 4902. 10.1038/s41598-019-41277-z. [PubMed: 30894629]

80. Chen M, Horn HT, Wen T, Cryns VL, and Anderson RA (2021). Assessing In Situ Phosphoinositide-Protein Interactions Through Fluorescence Proximity Ligation Assay in Cultured Cells. Methods Mol Biol 2251, 133–142. 10.1007/978-1-0716-1142-5_9. [PubMed: 33481236]

Highlights

- Under steady state, DELE1 is degraded by matrix-resident LONP1 soon after import.
- DELE1 import is arrested in iron deficiency, which stabilizes it on mitochondria.
- The stabilized DELE1 full-length form activates HRI at the mitochondrial surface.
- DELE1-HRI-ISR protects erythroid cells from iron deficiency-induced cell death.

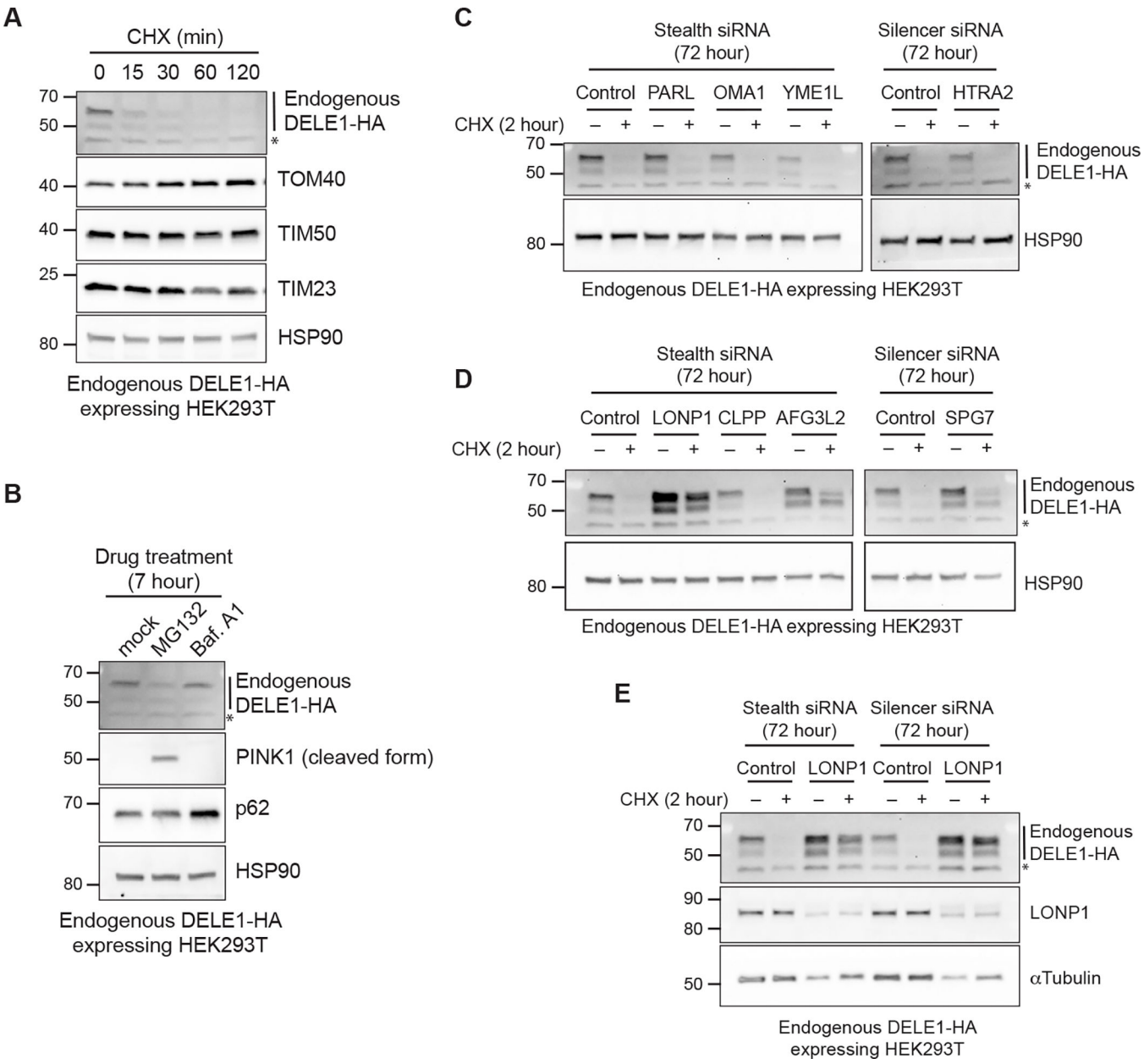

Figure 1. DELE1 is a short-lived protein that is degraded by LONP1 after mitochondrial import.

(A) Endogenous DELE1-HA expressing HEK293T cells were treated with cycloheximide (CHX) for the indicated time periods. Cell lysates were analyzed by immunoblotting (IB) with the indicated antibodies. HSP90 is shown as a loading control.

(B) IB for lysates of endogenous DELE1-HA HEK293T cells treated with MG132 or Bafilomycin A1 (Baf. A1) for 7 hours.

(C-E) IB for lysates of endogenous DELE1-HA HEK293T cells transfected with the indicated siRNAs for 72 hours and treated with CHX for the last 2 hours before harvest.

*; non-specific bands.

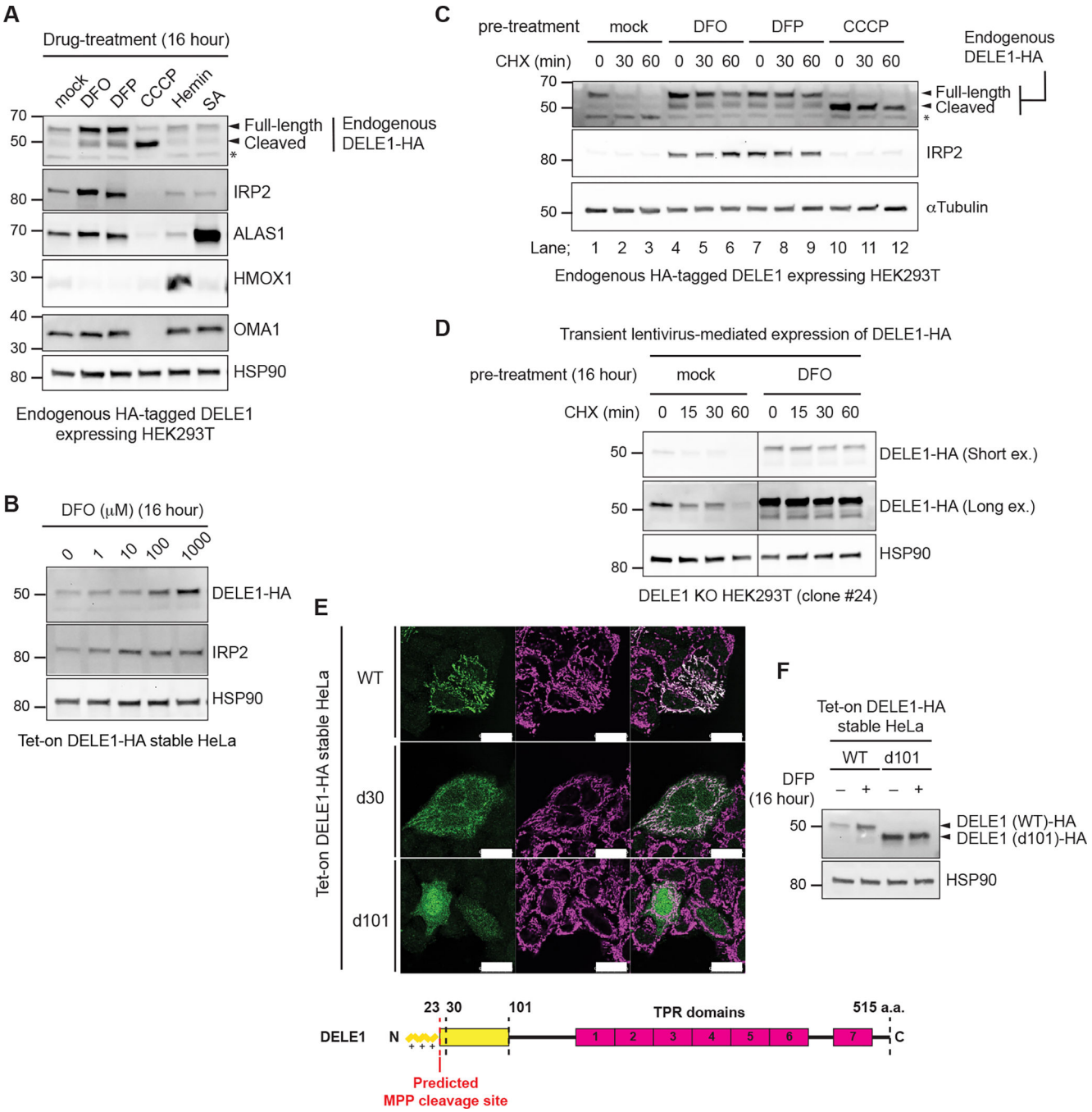

Figure 2. Iron deficiency stabilizes DELE1.

(A) Endogenous DELE1-HA HEK293T cells were treated with Deferoxamine (DFO), Deferiprone (DFP), CCCP, Hemin or succinyl acetone (SA) for 16 hours. The lysates were analyzed by immunoblotting (IB) with the indicated antibodies.

(B) IB for lysates of tet-on DELE1-HA stable HeLa cells treated with the indicated concentration of DFO for 16 hours. Doxycycline was added 8 hours prior to DFO treatment to induce the expression of DELE1-HA.

(C) IB for lysates of endogenous DELE1-HA HEK293T cells pre-treated with either DFO, DFP for 16 hours, or CCCP for 1.5 hours, and subsequently subjected to the CHX chase at the indicated time periods.
(D) HEK293T DELE1 knockout (KO) cells (clone #24) were transiently infected with lentivirus expressing DELE1-HA. After 24 hours, cells were treated with DFO for 16 hours and were subsequently subjected to the CHX chase at the indicated time periods. Cell lysates were analyzed by IB.
(E) Immunocytochemistry (ICC) for Tet-on DELE1 (wild-type, WT)-HA, DELE1 (delta 30, d30)-HA, DELE1 (delta 101, d101)-HA stable HeLa cells. Scale bars; 25 μm. A schematic representation of the domain structure of DELE1 is shown at the bottom.
(F) IB for lysates of tet-on DELE1 WT-HA or DELE1 d101-HA stable HeLa cells were treated with DFP for 16 hours. Doxycycline was added 8 hours prior to DFO treatment to induce the expression of DELE1 WT-HA or DELE1 d101-HA.
See also Figure S1.

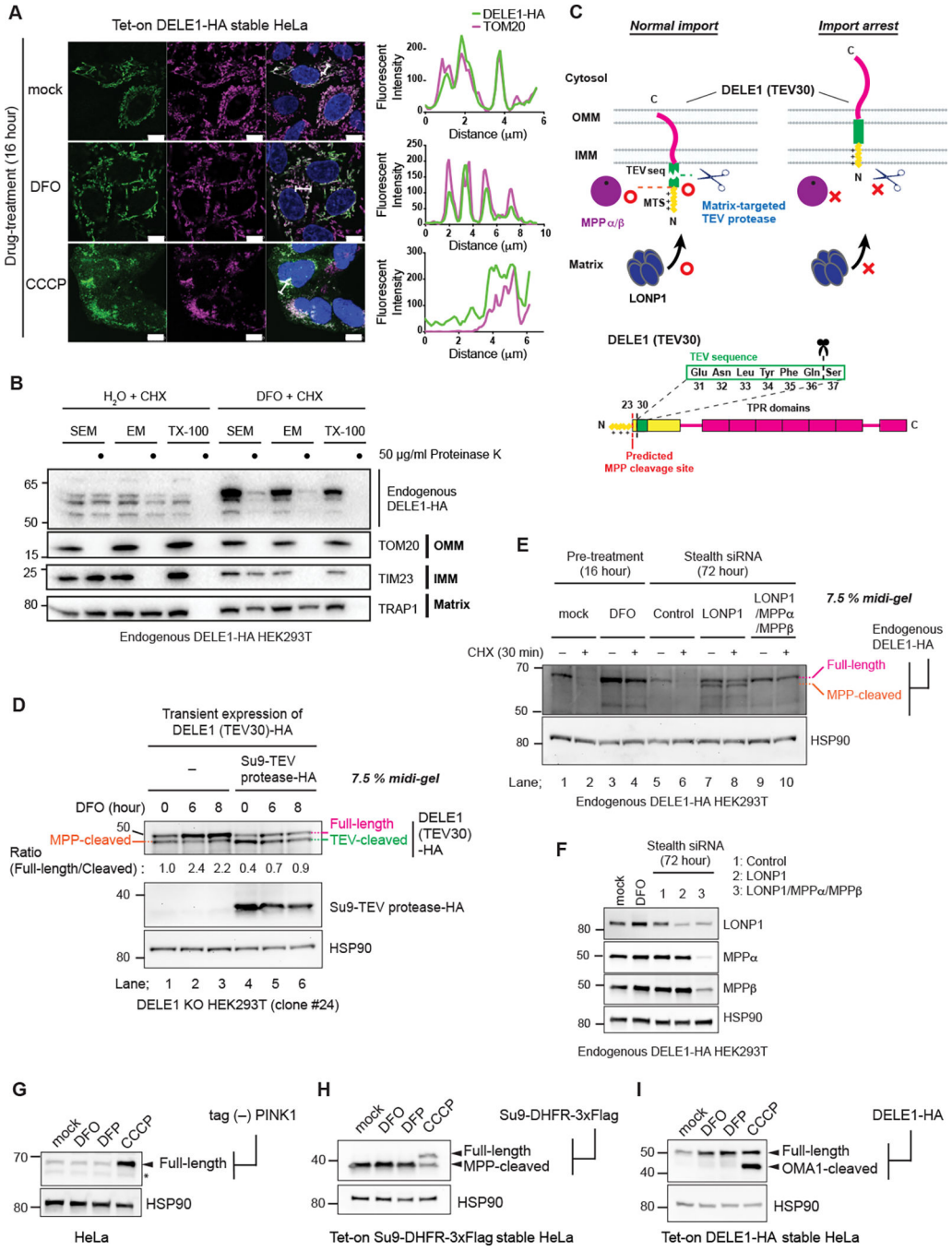

Figure 3. DELE1 is stabilized on mitochondria by an iron deficiency-dependent mitochondrial import arrest.

(A) Tet-on DELE-HA stable HeLa cells were treated with DFO or CCCP for 16 hours. The subcellular localization of DELE1-HA was determined by immunocytochemistry (ICC). Scale bars; 10 μm. Line profiles for the indicated fluorescent intensities determined along the white lines are shown to the right. (B) Crude mitochondrial fractions were isolated from Endogenous DELE1-HA HEK293T cells that were treated with CHX for 30 min with or without the pre-treatment with DFO for 16 hours, and were subjected to *in vitro* proteinase K protection assay at the indicated proteinase K concentration in the indicated

buffer conditions. Sensitivities of endogenous DELE1-HA and other mitochondrial marker proteins to proteinase K were determined by immunoblotting (IB).

(C) Schematic representation for the TEV cleavage assay. Suppression of the proteases-mediated cleavage of DELE1 by import arrest (upper panel). Insertion of the TEV cleavage sequence after the predicted MPP cleavage site of DELE1 [DELE1(TEV30)] (lower panel).

(D) DELE1 KO cells were transfected with the TEV sequence-inserted DELE1 (DELE1(TEV30)-HA) with or without the matrix-targeted TEV protease (Su9-TEV protease-HA). After 24 hours, cells were treated with DFO for the indicated time periods. Cell lysates were separated in an SDS-PAGE 7.5% polyacrylamide Midi gel and analyzed by IB.

(E) IB for lysates of endogenous DELE1-HA HEK293T cells treated with CHX for 30 min with or without pre-treatment of DFO for 16 hours (lane 1–4), or transfected with the indicated siRNAs for 72 hours, and subsequently treated with CHX for 30 min (lane 5–10).

(F) Knockdown efficiency of indicated proteins in (E) determined by IB.

(G to I) HeLa cells transiently transfected with tag (−) PINK1 (G), Tet-on Su9-DHFR-3xFlag stable HeLa cells (H), or Tet-on DELE1-HA stable HeLa cells (I), were treated with DFO, DFP or CCCP for 16 hours. Doxycycline was added 8 hours prior to DFO treatment to induce the expression of Su9-DHFR-3xFlag (H) or DELE1-HA (I). Cell lysates were analyzed by IB. *; non-specific bands.

See also Figure S2.

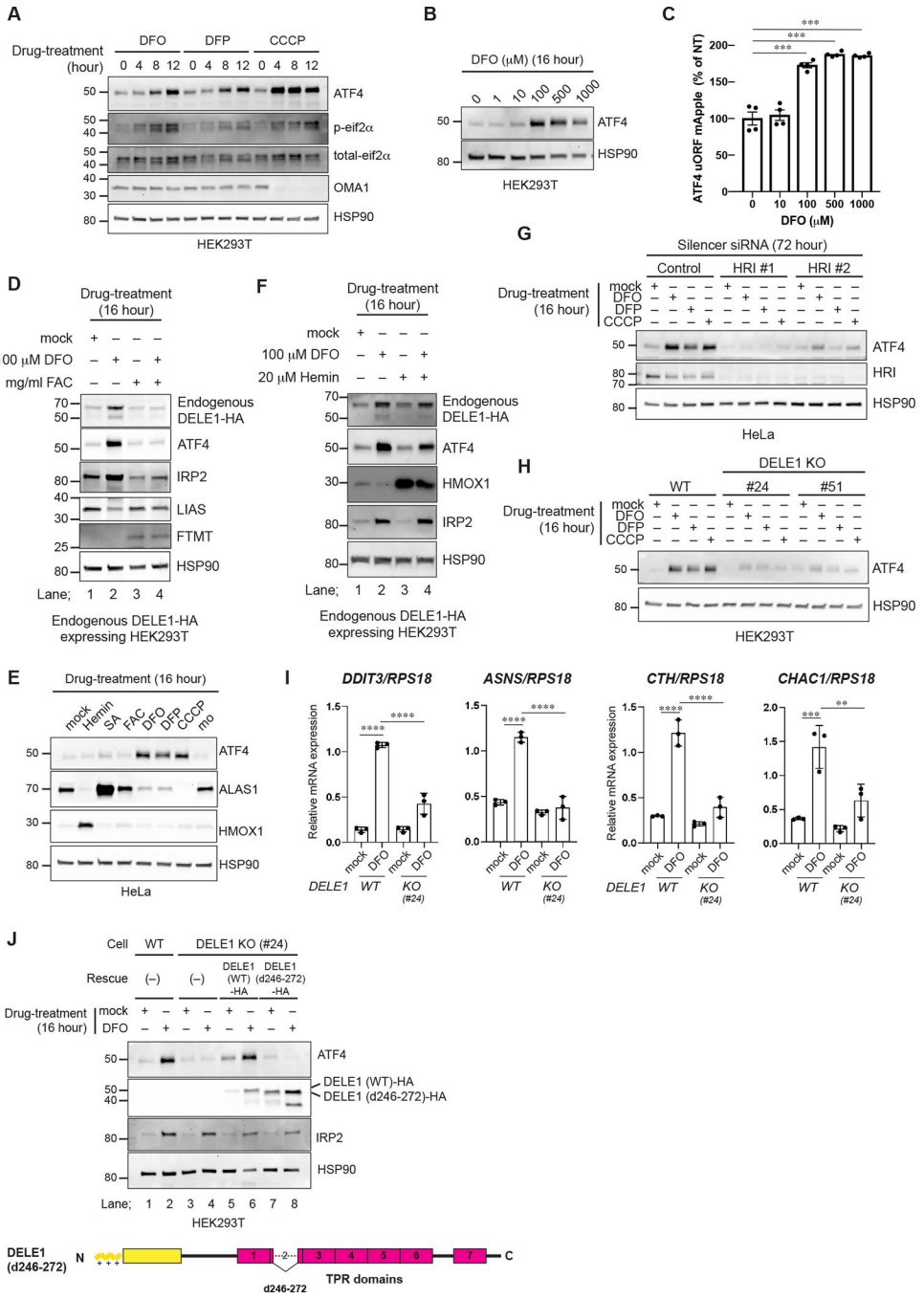

Figure 4. DELE1 activates an HRI-mediated ISR following iron deficiency.

(A, B) HEK293T cells were treated with DFO, DFP or CCCP for the indicated time periods (A) or were treated with the indicated concentrations of DFO for 16 hours (B). Cell lysates were analyzed by immunoblotting (IB) with the indicated antibodies.

(C) ATF4 reporter (ATF4 uORF mApple)-expressing HeLa cells were treated with the indicated concentrations of DFO for 16 hours and were subjected to flow cytometry analysis. Data are shown as mean ± S.D. (N=4). ***P = 0.0001 (One-way ANOVA followed by Dunnett's multiple comparison's test).

(D) IB for lysates of endogenous DELE1-HA HEK293T cells treated with DFO with or without ferric ammonium citrate (FAC) for 16 hours.
(E) IB for lysates of HeLa cells treated with the indicated compounds for 16 hours.
(F) IB for lysates of endogenous DELE1-HA HEK293T cells treated with DFO for 16 hours in the presence or absence of hemin.
(G) IB for lysates of HeLa cells transfected with indicated siRNAs for 72 hours, and treated with DFO, DFP, or CCCP for the last 16 hours.
(H) IB for lysates of HEK293T WT or DELE1 KO cell lines (clone #24 and #51) treated with DFO, 1 mM DFP, or CCCP for 16 hours. The lysates were analyzed by IB.
(I) Quantitative PCR for ISR target gene expression in HEK293T WT or DELE1 KO (clone #24) cells treated with DFO for 16 hours. Shown are mean ± S.D. (N=3). **** $P<0.0001$, *** $P<0.001$, and ** $P<0.01$ (One-way ANOVA followed by Turkey's multiple comparison).
(J) DELE1(WT)-HA or DELE1(d246–272)-HA was expressed in DELE1 KO HEK293T cells (clone #24) through lentivirus infection for 40 hours. Cells were treated with DFO for the last 16 hours before harvest. Cell lysates were analyzed by IB.
See also Figure S3.

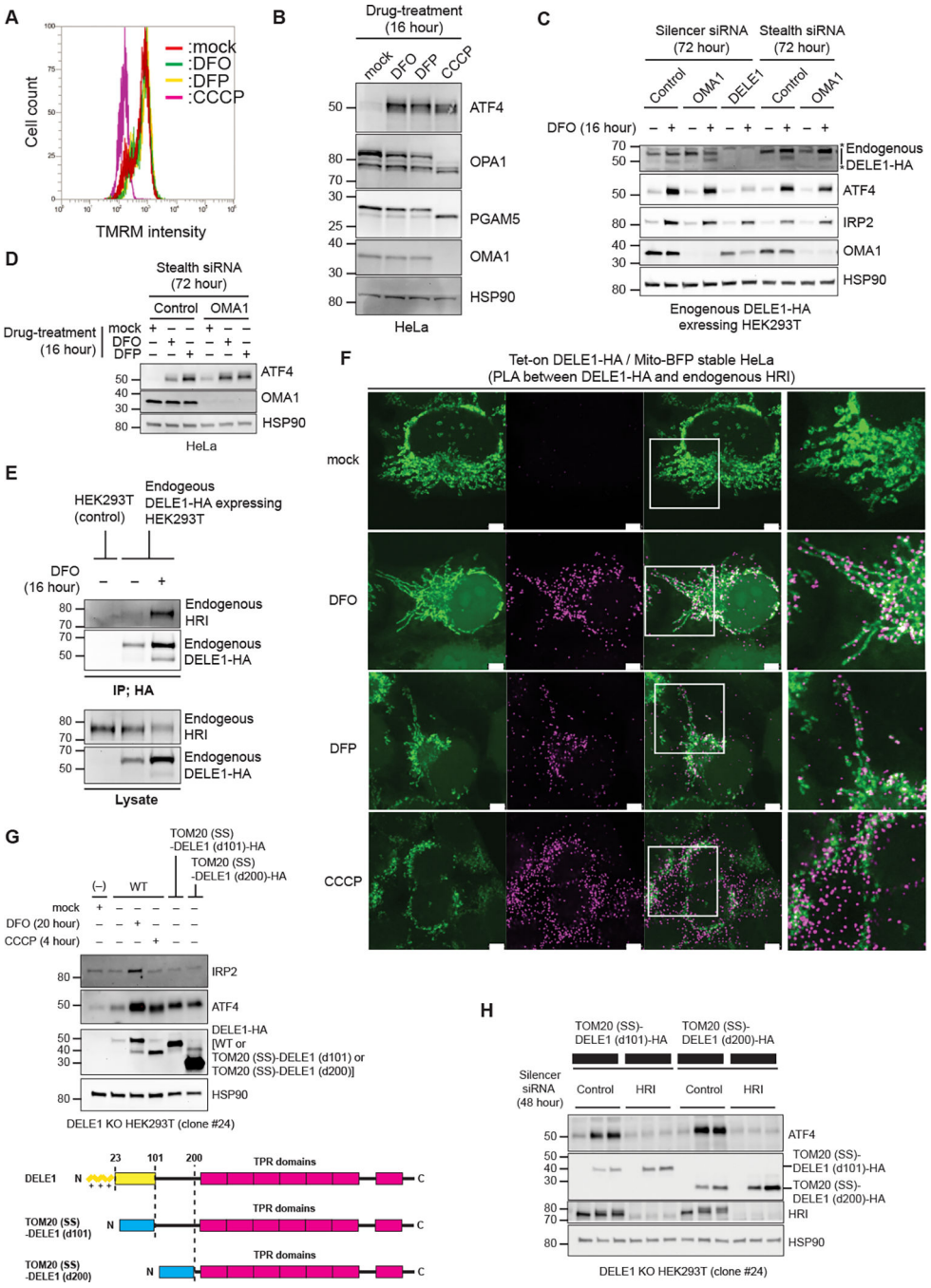

Figure 5. DELE1 on mitochondrial surface activates HRI.

(A) Flow cytometry analysis to determine mitochondrial membrane potential in HeLa cells treated with either DFO, DFP or CCCP for 16 hours, and with TMRM for the last 15 min.

(B) HeLa cells were treated with either DFO, DFP or CCCP for 16 hours. Cell lysates were analyzed by immunoblotting (IB) with the indicated antibodies.

(C, D) IB for lysates of endogenous DELE1-HA HEK293T cells (C) or HeLa cells (D) transfected with indicated siRNAs for 72 hours, and treated with DFO or DFP for the last 16 hours before harvest. *; non-specific bands.

(E) Endogenous DELE1-HA was immunoprecipitated with anti-HA antibody from the indicated HEK293T cells with or without 16 hours of DFO treatment. The samples were subjected to IB. IP; immunoprecipitation.

(F) Proximity Ligation Assay (PLA) between overexpressed DELE1-HA and endogenous HRI. Tet-on DELE1-HA stable HeLa cells that stably express Mito-BFP were treated with DFO or DFP for 20 hours, or CCCP for 4 hours, under Doxycycline-added conditions, and were subjected to PLA. White arrow heads indicate representative PLA signals that were observed exactly on or close proximity to mitochondria. Scale bars; 5 μm. Magnified merge images of the squared area are shown to the right. Low magnification images are shown in Figure S4A.

(G) DELE1-HA or the OMM-tethered DELE1 [TOM20(SS)-DELE1(d101)-HA] or TOM20(SS)-DELE1(d200)-HA] was expressed in DELE1 KO HEK293T cells (clone #24) through lentivirus infection for 44 hours. Cells were treated with DFO for the last 20 hours or CCCP for the last 4 hours before harvest. Cell lysates were analyzed by IB (upper panel). Schematic representation of TOM20(SS)-DELE1(d101)-HA and TOM20(SS)-DELE1 (d200)-HA (lower panel). The OMM-targeting signal of TOM20 is shown as a blue box.

(H) IB for lysates of DELE1 KO HEK293T cells transfected with indicated siRNAs for 48 hours, and infected with the OMM-tethered DELE1-HA-expressing lentiviruses for the last 24 hours before harvest.

See also Figure S4.

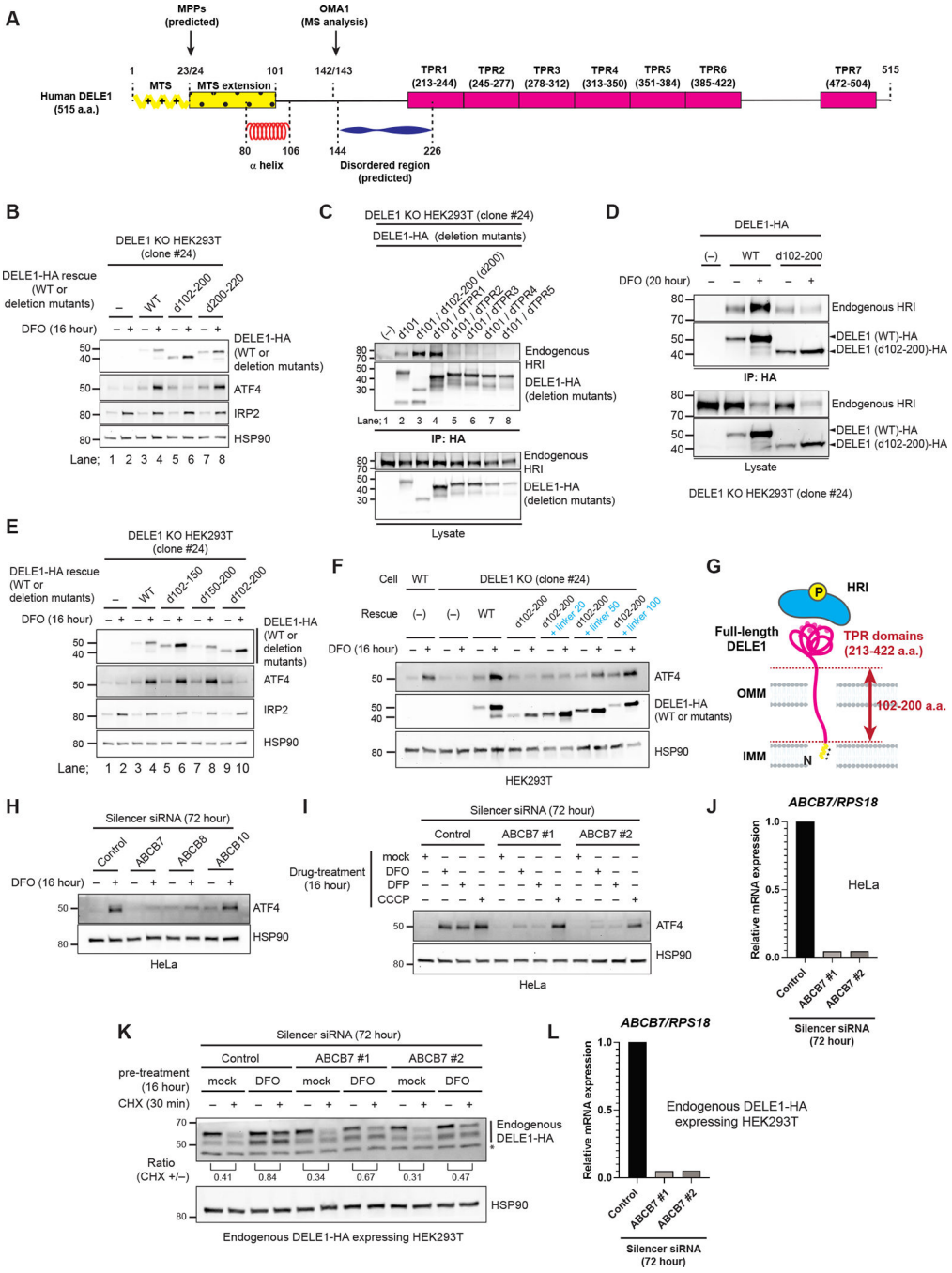

Figure 6. Determination of critical factors that are required for the iron deficiency-induced ISR activation.

(A) A schematic representation of DELE1 domain structures. See text for details.

(B) DELE1 (WT) or DELE1 deletion mutants that lacked indicated regions were expressed in DELE1 KO HEK293T cells through lentivirus infection for 40 hours. Cells were treated with DFO for the last 16 hours before harvest. Cell lysates were analyzed by immunoblotting (IB).

(C) The indicated DELE1 deletion mutants were transiently transfected in DELE1 KO HEK293T cells. After 24 hours, cells were lysed and each DELE1 was immunoprecipitated with anti-HA antibody. The samples were subjected to IB. IP; immunoprecipitation.
(D) DELE1 WT or d102-200 were transiently infected in DELE1 KO HEK293T cells (clone #24). Cells were subsequently treated with DFO for the last 20 hours before harvest. Each DELE1 was immunoprecipitated with anti-HA antibody. Samples were subjected to IB.
(E, F) DELE1 WT or DELE1 deletion mutants that lacked indicated regions (E) or linker-inserted DELE1(d102-200) mutants (F) were expressed in DELE1 KO HEK293T cells through lentivirus infection for 40 hours. Cells were treated with DFO for the last 16 hours before harvest. Cell lysates were analyzed by IB.
(G) A model for the role of 102–200 a.a. region of DELE1 in HRI activation during iron deficiency. See text for details.
(H) IB for lysates of HeLa cells transfected with indicated siRNAs for 72 hours, and treated with DFO for the last 16 hours.
(I) IB for lysates of HeLa cells transfected with indicated siRNAs for 72 hours, and treated with DFO, DFP, or CCCP for the last 16 hours.
(J) Knockdown efficiency of ABCB7 in (I) determined by quantitative PCR (qPCR).
(K) Endogenous DELE1-HA HEK293T cells were transfected with indicated siRNAs for 72 hours. Cells were treated with DFO for 16 hours, followed by the CHX chase for the last 30 min before harvest. Cell lysates were analyzed by IB. *; non-specific bands.
(L) Knockdown efficiency of ABCB7 in (K) determined by qPCR.
See also Figure S5 and Figure S6.

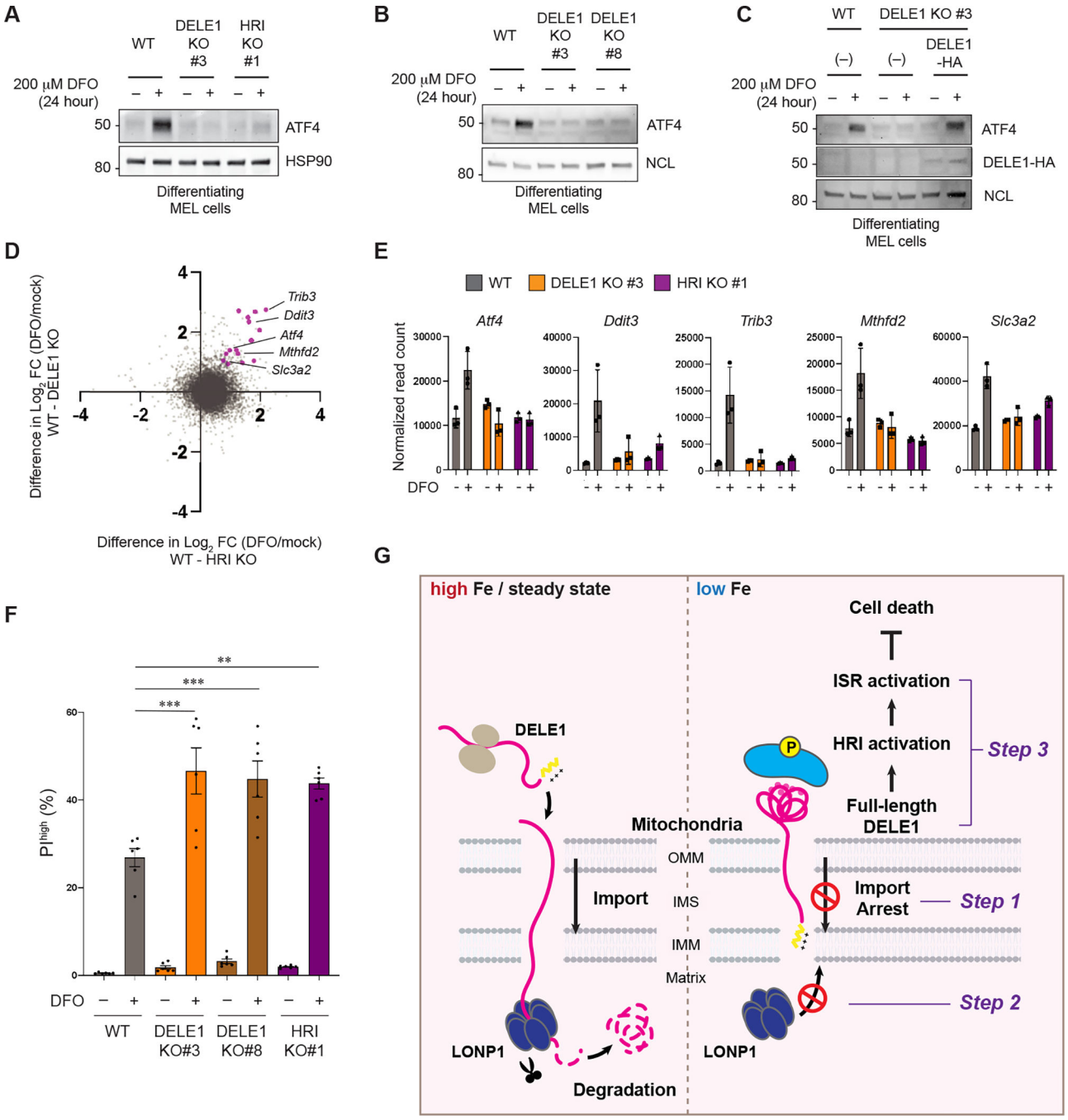

Figure 7. DELE1-HRI-ISR pathway protects the erythropoietic cell lineage against ferroptosis.

(A, B) MEL wildtype (WT), two independent DELE1 KO (clone #3 and clone #8), and HRI KO (clone #1) cells were cultured with 2% DMSO-containing medium in the presence or absence of DFO for 24 hours. Cell lysates were analyzed by immunoblotting (IB) with the indicated antibodies. HSP90 in (A) and NCL in (B) are shown as loading controls.

(C) IB for lysates of WT, DELE1 KO, or DELE1(WT)-HA-transfected DELE1 KO MEL cells. Cells were treated with DFO for the last 24 hours before harvest.

(D) MEL WT, DELE1 KO, and HRI KO cells were cultured with 2% DMSO-containing medium in the presence or absence of DFO for 24 hours. Cell lysates were subjected to RNA sequencing analysis. Differences between WT and HRI KO (X axis) or WT and DELE1 KO (Y axis) in $\log_2$ fold changes (FC) of each gene expression before and after iron chelation (DFO/mock) are plotted. Representative ISR target genes are shown in magenta.
(E) Relative mRNA expression of representative ISR target genes selected from the RNA sequencing data.
(F) MEL WT, DELE1 KO (clone #3 and #8), and HRI KO (clone #1) cells were cultured with 2% DMSO-containing medium in the presence or absence of DFO for 48 hours. Dead cells were determined by flow cytometry for Propidium iodide (PI) positive cells. Data are shown as mean ± S.D. (N=5–6). ***P<0.001 and **P<0.01 (One-way ANOVA followed by Turkey's multiple comparison).
(G) A proposed model of the iron-deficiency-induced mitochondrial import regulation of DELE1 and the subsequent activation of the HRI-ISR pathway. See text for details.
See also Figure S7.

Key resources table

REAGENT or RESOURCE	SOURCE	IDENTIFIER
Antibodies		
HA	Cell Signaling	2367S; RRID:AB_10691311
TOM40	Proteintech	18409-1-AP; RRID:AB_2303725
TIM50	Santa Cruz	sc-393678; RRID:AB_2714191
TIM23	BD Biosciences	611222; RRID:AB_398754
HSP90	Santa Cruz	sc-7947; RRID:AB_2121235
HSP90	Cell Signaling	4874S; RRID:AB_2121214
PINK1	Cell Signaling	6946S; RRID:AB_11179069
p62	Abcam	ab56416; RRID:AB_945626
LONP1	Proteintech	66043-1-lg; RRID:AB_2881494
LONP1	Novus Biologicals	NBP1-81734; RRID:AB_11002818
αTubulin	Sigma	T6199; RRID:AB_477583
IRP2	Cell Signaling	37135S; RRID:AB_2799110
ALAS1	Abcam	ab154860
HMOX1	GeneTex	GTX101147; RRID:AB_1950502
OMA1	Santa Cruz	sc-515788; RRID:AB_2905488
TOM20	Santa Cruz	sc-17764; RRID:AB_628381
MPPα	Sigma	HPA021648; RRID:AB_1855491
MPPβ	Proteintech	16064-1-AP; RRID:AB_2167122
M2	Sigma	F1804; RRID: AB_262044
ATF4	Cell Signaling	11815S; RRID:AB_2616025
phospho-eif2α	Cell Signaling	3398; RRID:AB_2096481
total-eif2α	Cell Signaling	5324; RRID:AB_10692650
LIAS	Proteintech	11577-1-AP; RRID:AB_2135972
SDHB	Proteintech	10620-1-AP; RRID:AB_2285522
PPAT	Proteintech	15401-1-AP; RRID:AB_2166532
FTMT	Abcam	ab66111
OPA1	BD Biosciences	612607; RRID:AB_399889
PGAM5	Thermo Fisher Scientific	PA5-57894; RRID:AB_2645430
HRI	Proteintech	20499-1-AP; RRID:AB_10697665
ISCU	Proteintech	14812-1-AP; RRID:AB_2280362
NCL	Cell Signaling	14574; RRIS:AB_2798519
TRAP1	Cell Signaling	92345: RRID:AB_2800183
Bacterial and virus strains		
N/A		
Biological samples		
N/A		
Chemicals, peptides, and recombinant proteins		

REAGENT or RESOURCE	SOURCE	IDENTIFIER
Cycloheximide (CHX)	Cayman Chemical	14126
MG132	Sigma	C2211
Bafilomycin A1 (Baf. A1)	Cayman Chemical	11038
Deferoxamine (mesylate) (DFO)	Cayman Chemical	14595
Deferiprone (DFP)	Cayman Chemical	20387
CCCP	Sigma	C2759
Hemin chloride	Cayman Chemical	16487
Succinyl acetone (SA)	MedChemExpress	HY-W010184
Proteinase K	Sigma	P6556
Ferric ammonium citrate (FAC)	Sigma	RES20400-A7
Erastin	Cayman Chemical	17754
trans-ISRIB	Cayman Chemical	16258
Doxycycline	Sigma	D9891
DSP (dithiobis(succinimidyl propionate))	Thermo Fisher Scientific	22585
X-tremeGENE 9 DNA transfection reagent	Roche	6365787001
Lipofectamine RNAi max transfection reagent	Thermo Fisher Scientific	13778075
Tetramethylrhodamine, Methyl Ester, Perchlorate (TMRM)	Thermo Fisher Scientific	T668
Critical commercial assays		
Duolink In Situ PLA Probe Starter Kit	Sigma	DUO92101
Deposited data		
Raw images	This study	Mendeley Data (DOI: 10.17632/7p8w52928v.1)
RNA seq data	This study	SRA (accession number: PRJNA970328)
Experimental models: Cell lines		
HEK293T	ATCC	CRL-3216
HeLa	ATCC	CCL-2.2
Endogenous DELE1-HA HEK293T	Fessler et al., 2020	N/A
Tet-on DELE1-HA stable HeLa	Houston et al., 2021	N/A
Tet-on Su9-DHFR-3xFlag stable HeLa	Sekine et al., 2019	N/A
DELE1 KO HEK293T clone #24	This study	N/A
DELE1 KO HEK293T clone #51	This study	N/A
ATF4_uORF_mApple-stable HeLa	This study	N/A
Tet-on DELE1-HA / Mito-BFP stable HeLa	This study	N/A
MEL	Millipore Sigma	F4N
DELE1 KO MEL clone #3	This study	N/A
DELE1 KO MEL clone #8	This study	N/A
HRI KO MEL clone #1	This study	N/A
Experimental models: Organisms/strains		
N/A		
Oligonucleotides		

REAGENT or RESOURCE	SOURCE	IDENTIFIER
Stealth RNAi Negative Control Med GC Duplex #2	Thermo Fisher Scientific	12935112
Silencer Select Negative Control #1 siRNA	Thermo Fisher Scientific	4390843
Stealth RNAi PARL	Thermo Fisher Scientific	HSS183080
Stealth RNAi OMA1	Thermo Fisher Scientific	HSS132976
Stealth RNAi YME1L	Thermo Fisher Scientific	HSS116546
Stealth RNAi HtrA2	Thermo Fisher Scientific	HSS146986
Stealth RNAi LONP	Thermo Fisher Scientific	HSS113887
Silencer Select LONP #1	Thermo Fisher Scientific	s17902
Silencer Select LONP #2	Thermo Fisher Scientific	s17903
Stealth RNAi CLPP	Thermo Fisher Scientific	HSS112033
Stealth RNAi AFG3L2	Thermo Fisher Scientific	HSS116886
Stealth RNAi SPG7	Thermo Fisher Scientific	HSS110137
Stealth RNAi MPPa	Thermo Fisher Scientific	HSS118357
Stealth RNAi MPPb	Thermo Fisher Scientific	HSS114169
Silencer Select HRI #1	Thermo Fisher Scientific	s25822
Silencer Select HRI #2	Thermo Fisher Scientific	s25823
Silencer Select DELE1 #1	Thermo Fisher Scientific	s18966
Silencer Select DELE1 #2	Thermo Fisher Scientific	s18967
Silencer Select ABCB7 #1	Thermo Fisher Scientific	s855
Silencer Select ABCB7 #2	Thermo Fisher Scientific	s857
Silencer Select ABCB8	Thermo Fisher Scientific	s22104
Silencer Select ABCB10	Thermo Fisher Scientific	s23857
Silencer Select ISCU #1	Thermo Fisher Scientific	s23909
Silencer Select ISCU #2	Thermo Fisher Scientific	s23908
Recombinant DNA		
pLVX-puro-DELE1-HA	Houston et al., 2021	N/A
pLVX-puro-DELE1 (TEV30)-HA	This study	N/A
pcDNA3.1 (+) Su9-TEV protease-HA	Sekine et al., 2019	N/A
pRetroX-Tight-Pur-DELE1-HA	Houston et al., 2021	N/A
pRetroX-Tight-Pur-DELE1(d30) -HA	This study	N/A
pRetroX-Tight-Pur-DELE1(d101)-HA	This study	N/A
pRetroX-Tight-Pur-pSu9-DHFR-tev-3xFlag	Sekine et al., 2019	N/A
pCMV (d1) PINK1 (Tag-)	Okatsu et al., 2012	N/A
pLVX-puro-PINK1-HA	This study	N/A
lentiCRISPR v2-hygro-human DELE1 (Guide#1)	This study	N/A
lentiCRISPR v2-hygro-human DELE1 (Guide#2)	This study	N/A
pXG237	Guo et al., 2020	Addgene #141281
pLVX-puro-DELE1(d246-272)-HA	This study	N/A
pLVX-puro-TOMM20(ss)-DELE1(d101)-HA	This study	N/A

REAGENT or RESOURCE	SOURCE	IDENTIFIER
pLVX-puro-TOMM20(ss)-DELE1(d200)-HA	This study	N/A
pLVX-puro-DELE1(d102-200)-HA	This study	N/A
pLVX-puro-DELE1(d200-220)-HA	This study	N/A
pLVX-puro-DELE1(d101)-HA	This study	N/A
pLVX-puro-DELE1(d101/d102-200)-HA	This study	N/A
pLVX-puro-DELE1(d101/dTPR1)-HA	This study	N/A
pLVX-puro-DELE1(d101/dTPR2)-HA	This study	N/A
pLVX-puro-DELE1(d101/dTPR3)-HA	This study	N/A
pLVX-puro-DELE1(d101/dTPR4)-HA	This study	N/A
pLVX-puro-DELE1(d101/dTPR5)-HA	This study	N/A
pLVX-puro-DELE1(d102-150)-HA	This study	N/A
pLVX-puro-DELE1(d150-200)-HA	This study	N/A
pLVX-puro-DELE1(d102-200 + linker 20)-HA	This study	N/A
pLVX-puro-DELE1(d102-200 + linker 50)-HA	This study	N/A
pLVX-puro-DELE1(d102-200 + linker 100)-HA	This study	N/A
lentiCRISPR v2-puro-mouse DELE1(Guide#1)	This study	N/A
lentiCRISPR v2-puro-mouse DELE1 (Guide#2)	This study	N/A
lentiCRISPR v2-puro-mouse HRI (Guide#1)	This study	N/A
lentiCRISPR v2-puro-mouse HRI (Guide#2)	This study	N/A
Mito-BFP	Friedman et al., 2011	Addgene #49151
pLVX-puro-DELE1(d80-106)-HA	This study	N/A
pLVX-puro-PINK1(MTS)-DELE1(d101)-HA	This study	N/A
pLVX-puro-DELE1(dTPR1-7)-HA	This study	N/A
pLVX-puro	Clontech	632164
pRetroX-Tight-Pur	Clontech	632104
pRetroX-Tet-On Advanced	Clontech	632104
lentiCRISPR v2-puro	Sanjana et al., 2014	Addgene #52961
lentiCRISPR v2-hygro	Stringer et al., 2019	Addgene #98291
Software and algorithms		
BioRender	N/A	https://app.biorender.com/user/signin
Other		
N/A		